Double resonance Raman spectra of graphene: a full 2D calculation

by

Rohit Narula

Submitted to the Department of Materials Science and Engineering in partial fulfillment of the requirements for the degree of

Master of Science in Materials Science and Engineering

at the

MASSACHUSETTS INSTITUTE OF TECHNOLOGY

September 2007

Author.....
Department of Materials Science and Engineering
August 13, 2007

Certified by.....
Stephanie Reich
Visiting Assistant Professor of Materials Science and Engineering

Certified by.....
Francesco Stellacci
Finmeccanica Associate Professor of Materials Science and Engineering

Accepted by.....
Samuel M. Allen
POSCO Professor of Physical Metallurgy
Chairman, Department Committee on Graduate Students

Double resonance Raman spectra of graphene: a full 2D calculation

By

Rohit Narula

Submitted to the Department of Materials Science and Engineering

on August 10, 2007, in partial fulfillment of the requirements for the degree of

Master of Science in Materials Science and Engineering

Abstract

Visible range Raman spectra of graphene are generated based on the double resonant process employing a full two-dimensional numerical calculation applying second-order perturbation theory. Tight binding expressions for both the TO phonon dispersion and the $\pi - \pi^*$ electronic bands are used, which are then fit to experimental or ab-initio results. We are able to reproduce the single-peak D mode of graphene at $\sim 1380\ cm^{-1}$ that is identical to experiment. A near linear shift in the D mode peak with changing incoming laser energy of $33\ cm^{-1}/eV$ is calculated. Our shift marginally underestimates the experimental shifts as most of the literature features specimens that contain a few or more layers of graphene through to graphite that ought to subtly alter their electronic and phonon dispersions. However, our approach is readily applicable to such homologous forms of graphene once we have available their electronic band structure and phonon dispersions.

Thesis Supervisor: Stephanie Reich
Title: Visiting Assistant Professor of Materials Science and Engineering

Acknowledgements

A culmination of work done at MIT from September '06 till July '07, this thesis would not have been possible without the exemplary supervision of Prof. Stephanie Reich who introduced me to the hitherto beguiling world of carbon based materials and on whose original work much of this thesis builds upon. Her spell of becalming influence and effortless charm transformed what would otherwise have been an exercise in perseverance and loopy coding into a minor *juissance*. My parents, who have encored their biggest mistake by investing in my every hedonistic excess. Prof. Eugene Fitzgerald who maneuvered me to MIT and has continually inspired me with his vision and *joie de vivre*. Gabrielle Joseph, who cleaned-up in the wake of my frequent procrastinations and cheerfully indulges a most incipient humor. My lovely group mate Serena, who ultimately decided to endure by absentia before she bequeathed her privileges to the quartet of linux workhorses. But above all, to my solipsism that has contrived a most beautiful pomp and circumstance; I dedicate this thesis to thee.

1 Introduction

A single layer of carbon atoms in a hexagonal network –graphene, is a building block for carbon-based materials such as carbon nanotubes, graphite, fullerenes etc. Initially presumed to not exist in the free-state, graphene has recently been receiving renewed interest as a material owing to its recent isolation via exfoliation from graphite (1). It shows a host of interesting properties such as its semi-metallic nature which is extremely rare for films of atomic thickness, ballistic electronic transport at sub-micrometer dimensions at ambient temperatures (1), attracting researchers to its potential application as a replacement for copper interconnects (2), field effect (1) for FET applications, the anomalous quantum Hall effect (3), strong electron-phonon coupling etc.

In this thesis we will discuss the Raman spectra of single layer graphene based on a full two dimensional calculation that is performed numerically. We start by explaining the Raman spectra of graphite that is expected to be very similar to graphene.

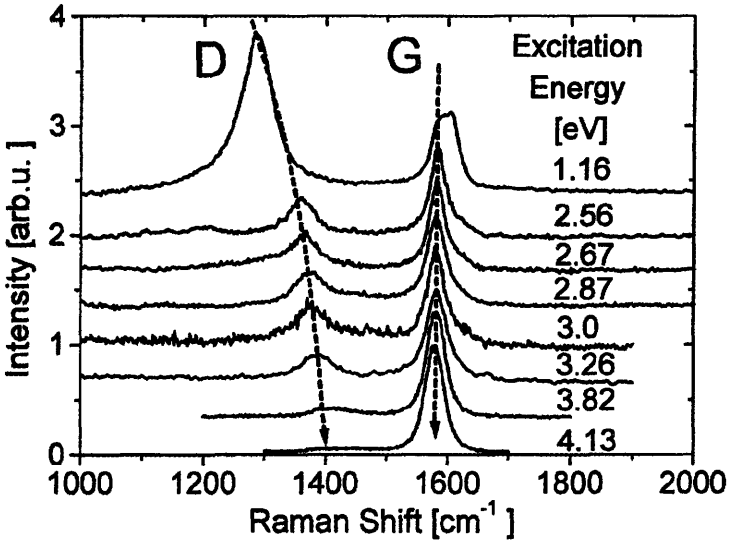

Figure 1-1: Raman spectra of graphite excited by laser lines with photon energies indicated. From Ref. (17).

The experimental Raman spectra of graphite shown in Figure 1-1 consists of a G band (also known as the Γ band) at 1589 cm^{-1} that remains stationary with changing excitation laser energy. On the other hand another peak known as the D peak (the D denoting defect) at ~1380 cm^{-1} shows an unexpected near-linear shift with excitation energy. The double resonant process as proposed by Thomsen and Reich in Ref. (4), is successful in explaining the Raman spectra of sp^2 bonded carbon-based materials such as graphene, graphite, carbon nanotubes etc. In the language of perturbation theory, the double resonant process is characterized by having two real intermediate states and provides a firm theoretical basis for the hitherto unexplained phenomena of the shift in the defect-related D mode of graphene with change in excitation laser energy.

Recent experimental measurements on graphene (see Ref. (5)) contrasted graphite's double-peak structure (the curve was fit to two Lorentzians) with a single peak structure for graphene as shown in Figure 2.1-2. Indeed, even early calculations of the Raman spectra of graphene (5), showed a double-peak structure for the *D* mode in graphene which was not seen experimentally (6).

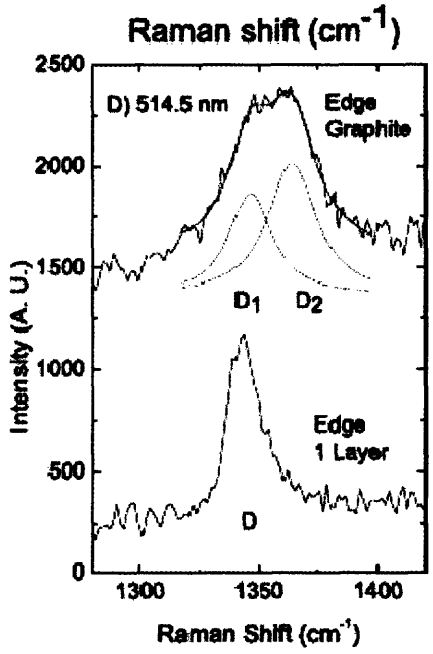

Figure 2.1-2: A comparison of the *D* mode peaks in the Raman spectra of graphite and graphene for excitation laser energy at 514 nm. From Ref. (6).

This thesis aims at extending the one dimensional model (See Ref. (4)) of the Raman spectra of graphene to a full 2-D calculation that is performed numerically.

It is able to recover the single-peak D mode evident in graphene and provides extensibility to multi-layer versions of graphene through to graphite.

Chapter 2 of this thesis sets the stage for our results by discussing the theoretical framework necessary for understanding the calculation required for generating the Raman spectra of graphene. Section 2.1 discusses the tight binding description of Graphene that is used to generate the electronic band gap and phonon dispersion whose constants are then fit to experimental or ab-initio data. Section 2.2 briefly develops basic perturbation theory and introduces Feynman diagrams that are used as an aid to visualize the double resonant process. The double resonant process is discussed at length in the context of graphene in section 2.3 and is followed by a section on selection rules and symmetry arguments that are used to explain the preponderant contribution of the TO phonon branch in the Raman spectra of graphene. Finally, in section 2.5, we describe the computational resources and complexity invoked via our numerical code.

Chapter 3 exposits the results of our calculations where we first discuss the calculation involving only the 1st nearest neighbor phonon dispersion in section 3.1, followed by section 3.2 that discusses the results based on a calculation that uses the more realistic 3rd nearest neighbor phonon dispersion. Finally, we present a discussion of our results in section 0 and finish with our conclusions and scope for future work.

2 Theoretical framework

2.1 Tight binding description of graphene

The electronic structure of any material is typically obtained by one of two approaches. The first, is generally known as the free electron approximation wherein the electrons are modeled to move essentially as free particles in a vanishingly small potential produced by the atoms and their interaction with other electrons. The second approach, in contrast to the first, is known as the tight binding or the linear combination of atomic orbitals (LCAO) approximation. Here we assume that the electrons are tightly bound to their nuclei and that when they are brought close to each other their wave functions overlap. Whereas in the free electron approach we model the electron wave functions as plane waves, in the tight binding approach we model them as atomic orbital wave functions. The interaction of the electronic states is what leads to the broadening of the eigenstates and their evolution into continuous bands of the solid. For graphene it is found that the tight binding approach is particularly successful in describing the band structure around the Fermi level.

The atomic number of carbon is 6 which leads to the ground-state orbital structure $1s^2 2s^2 2p^2$. However, in order for carbon to maximize the number of bonds for energy minimization, it's four valence electrons end up being distributed as one $2s$ electron and three $2p$ electrons. The overlap of the different electronic orbitals corresponding to each atom on the hexagonal network leads to the evolution of continuous electronic bands. The overlap between the p_z wave function with the s or the p_x and the p_y is strictly zero. While the s, p_x, and p_y wave functions are symmetric for points above and below the graphene layer, the p_z orbital changes sign. The contributions for positive and negative z cancel and the overlap vanishes on integrating over the entire space. Therefore, the p_z orbitals may be treated independently of the other valence electrons. These are found to be responsible for the π bonds of graphene (7), and are relevant whilst probing the electronic structure of graphene in the visible domain.

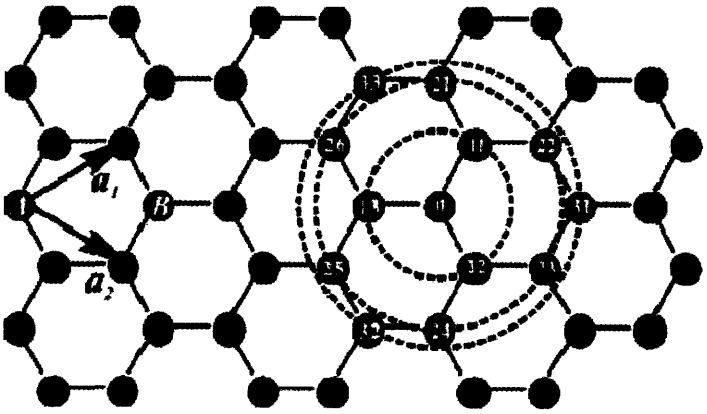

Figure 2.1-1: Hexagonal lattice of graphene. The sub-lattices are denoted by A and B. From Ref. (8)

Following the treatment and nomenclature found in Ref. (8); starting with the Schrodinger's Equation

$$H\psi(\boldsymbol{k}) = E(\boldsymbol{k})\psi(\boldsymbol{k}) \qquad 2.1.1$$

where H is the Hamiltonian, $E(\boldsymbol{k})$ are the energy eigenvalues at the wave vector $\boldsymbol{k}$, and $\psi(\boldsymbol{k})$ are the eigenfunctions. Writing these eigenfunctions as linear combination of Bloch functions $\Phi_l(\mathbf{k})$ we get

$$\psi(\boldsymbol{k}) = \sum_l C_l \, \Phi_l(\boldsymbol{k}) \qquad 2.1.2$$

The unit cell of graphene contains two carbon atoms, which are labeled A and B in Figure 2.1-1. With the normalized $2p_z$ orbitals of the isolated carbon atom denoted by $\varphi(\boldsymbol{r})$ we construct a Bloch function for the graphene sub lattice A.

$$\Phi_A = \frac{1}{\sqrt{N}} \sum_{R_A} e^{ik.R_A} \varphi(\boldsymbol{r} - \mathbf{R_A}) \qquad 2.1.3$$

and an equivalent function Φ_B for the second sub lattice, B. Here N is the number of unit cells in the solid and $\mathbf{R_A}$ is a lattice vector. The sum runs over all possible lattice vectors.

To solve Schrodinger's equation in Eq. (2.1.1) we substitute ψ with the linear combination of the Bloch functions in Eq. (2.1.2). Pre-multiplying both sides with Φ_A and Φ_B to form the matrix elements we obtain the system of linear equations

$$\begin{aligned} C_A[H_{AA}(\boldsymbol{k}) - E(\boldsymbol{k})S_{AA}(\boldsymbol{k}) + C_B[H_{AB}(\boldsymbol{k}) - E(\boldsymbol{k})S_{AB}(\boldsymbol{k})]] = 0 \\ C_A[H_{BA}(\boldsymbol{k}) - E(\boldsymbol{k})S_{BA}(\boldsymbol{k}) + C_B[H_{BB}(\boldsymbol{k}) - E(\boldsymbol{k})S_{BB}(\boldsymbol{k})]] = 0 \end{aligned} \qquad 2.1.4$$

Where H_{IJ} are the matrix elements of the Hamiltonian and S_{IJ} are the overlaps between the Bloch functions

$$H_{IJ} = < \Phi_I|H|\Phi_J >,\ S_{IJ} = < \Phi_I|\Phi_J > \qquad 2.1.5$$

We may simplify the Hamiltonian and overlap matrix by noting the equivalence of the A and B atoms in graphene. Therefore, the Hamiltonian matrix element H_{AA} given by the interaction of an atom at site A with itself and all other A atoms in the crystal is exactly the same as H_{BB}. Similarly, H_{BA} is simply the complex conjugate of H_{AB}. For the system of two linear equations in Eq. (2.1.4) to have a non-trivial

the determinant must vanish and therefore, the most general form of the secular equation for the π orbitals of graphene is

$$Det\begin{pmatrix} H_{AA}(\boldsymbol{k}) - E(\boldsymbol{k})S_{AA}(\boldsymbol{k}) & H_{AB}(\boldsymbol{k}) - E(\boldsymbol{k})S_{AB}(\boldsymbol{k}) \\ H_{AB}{}^{*}(\boldsymbol{k}) - E(\boldsymbol{k})S_{AB}{}^{*}(\boldsymbol{k}) & H_{AA}(\boldsymbol{k}) - E(\boldsymbol{k})S_{AA}(\boldsymbol{k}) \end{pmatrix} = 0 \qquad 2.1.6$$

The above determinant can be solved to yield

$$E(\boldsymbol{k})^{\pm} = \frac{-(-2E_0 + E_1) \mp \sqrt{(-2E_0 + E_1)^2 - 4E_2E_3}}{2E_3} \qquad 2.1.7$$

With

$$\begin{matrix} E_0 = H_{AA}(\boldsymbol{k}) - E(\boldsymbol{k})S_{AA}(\boldsymbol{k}) & E_1 = S_{AB}(\boldsymbol{k})H_{AB}{}^{*}(\boldsymbol{k}) + H_{AB}(\boldsymbol{k})S_{AB}{}^{*}(\boldsymbol{k}) \\ E_2 = H_{AA}(\boldsymbol{k})^2 - H_{AB}(\boldsymbol{k})H_{AB}{}^{*}(\boldsymbol{k}) & E_3 = S_{AA}(\boldsymbol{k})^2 - S_{AB}(\boldsymbol{k})S_{AB}{}^{*}(\boldsymbol{k}) \end{matrix} \qquad 2.1.8$$

$E(\boldsymbol{k})^{+}$ is the eigenvalue for the symmetric combination of the atomic wave functions also known as the valence band. Whereas the $E(\boldsymbol{k})^{-}$ is the antisymmetric conduction band.

Neglecting the overlap between wave functions centered at different atoms ($S_{AA} = 1; S_{AB} = 0$) E_1 vanishes and E_3 is equal to one. Equation (2.1.7) then simplifies to

$$E_{S=0}(\boldsymbol{k})^{\pm} = H_{AA}(\boldsymbol{k}) \mp |H_{AB}(\boldsymbol{k})| \qquad 2.1.9$$

2.1.1 1st nearest neighbor approximation

For the nearest neighbor interaction where every atom A in Figure 2.1-1 interacts with itself and the three atoms BB_{11}, BB_{12}, and BB_{13} causes H_{AA} to become constant; it reflects only the property of the A atom. Recalling that the π and π^* bands cross the K point at the Fermi level gives us

$$H_{AA} - |H_{AB}(K)| = H_{AA} + |H_{AB}(K)| = E_F = 0 \qquad 2.1.10$$

Or for the energies in the nearest neighbor approximation

$$E^{nn}{}_{S=0}(\boldsymbol{k})^{\pm} = \mp |H_{AB}(\boldsymbol{k})| \qquad 2.1.11$$

We calculate the matrix elements H_{IJ} and the overlap integrals S_{IJ} explicitly from the Bloch functions Φ_J in Eq. (2.1.3). For an atom A the matrix element H_{AA} is

$$H_{AA}(\boldsymbol{k}) = < \Phi_A|H|\Phi_{A'} >$$
$$H_{AA}(\boldsymbol{k}) = \frac{1}{N}\sum_{\mathbf{R_A}}\sum_{\mathbf{R_{A'}}} < e^{i\boldsymbol{k}.\mathbf{R_A}}\varphi(\boldsymbol{r}-\mathbf{R_A})|H|e^{i\boldsymbol{k}.\mathbf{R_{A'}}}\varphi(\boldsymbol{r}-\mathbf{R_{A'}}) > \qquad 2.1.12$$

The first sum runs over all N carbon atoms of type A in the graphene crystal. Considering only the nearest neighbors we note all three of them belong to the B sub lattice, see Figure 2.1-1. Thus, for a given $\mathbf{R_A}$ the second sum has only a single term, $\mathbf{R_{A'}} = \mathbf{R_A}$.

$$H_{AA}(\boldsymbol{k}) = \frac{1}{N}\sum_{\mathbf{R_A}} e^{i\boldsymbol{k}.(\mathbf{R_A}-\mathbf{R_A})} < \varphi_A(\boldsymbol{r}-\mathbf{R_A})|H|\varphi_A(\boldsymbol{r}-\mathbf{R_A}) > \qquad 2.1.13$$
$$= \varepsilon_{2p}$$

Empirical constants like ε_{2p}, are fit by comparing the empirical band structure to experimental or ab-initio results. S_{AA} is found in exactly the same way as H_{AA}. It is also constant, and we set it equal to one.

The matrix element between A and B atoms is given by the formal expression

$$H_{AB}(\boldsymbol{k}) = \frac{1}{N}\sum_{\mathbf{R_A}}\sum_{\mathbf{R_B}} e^{i\boldsymbol{k}.(\mathbf{R_B}-\mathbf{R_A})} < \varphi_A(\boldsymbol{r}-\mathbf{R_A})|H|\varphi_B(\boldsymbol{r}-\mathbf{R_B}) > \qquad 2.1.14$$

The second sum runs over all three nearest neighbors of a given atom A. The vectors $\mathbf{R_{1i}} = \mathbf{R_{B_{1i}}} - \mathbf{R_A}$ (i = 1,2,3) pointing from A to one of its neighbors B_{1i} can be found from Figure 2.1-1.

$$\mathbf{R_{11}} = \frac{1}{3}(2\mathbf{a_1} - \mathbf{a_2}),\ \mathbf{R_{12}} = \frac{1}{3}(-\mathbf{a_1} + 2\mathbf{a_2}),\ \mathbf{R_{13}} = \frac{1}{3}(-\mathbf{a_1} - \mathbf{a_2}), \qquad 2.1.15$$

We insert Eq. (2.1.15) into Eq. (2.1.14) and sum over the B neighbors and A atoms. There are three integrals of the form $< \varphi_A|H|\varphi_{B_{1i}} >$ in Eq. (2.1.14). These φ's exhibit radial symmetry in the graphene plane and the integral is found to depend only on the distance between atom A and B. As all three neighbors are equidistant, we may define a second adjustable constant γ_0 such that

$$H_{AB}(\boldsymbol{k}) = \frac{1}{N}(e^{i\boldsymbol{k}.\mathbf{R_{11}}} + e^{i\boldsymbol{k}.\mathbf{R_{12}}} + e^{i\boldsymbol{k}.\mathbf{R_{13}}}) < \varphi_A(\boldsymbol{r}-\mathbf{R_A})|H|\varphi_B(\boldsymbol{r}-\mathbf{R_A}-\mathbf{R_{11}}) >$$
$$H_{AB}(\boldsymbol{k}) = \gamma_0(1 + e^{i\boldsymbol{k}.\mathbf{a_1}} + e^{i\boldsymbol{k}.\mathbf{a_2}})e^{-\frac{1}{3}i\boldsymbol{k}.(\mathbf{a_1}+\mathbf{a_2})} \qquad 2.1$$

From Eq. (2.1.8) we obtain

$$E_2 = \varepsilon_{2p} - \gamma_0{}^2[2 + 2cos(\boldsymbol{k}.\mathbf{a_1}) + 2cos(\boldsymbol{k}.\mathbf{a_2}) + 2cos(\boldsymbol{k}.(\mathbf{a_1} - \mathbf{a_2})] \quad 2.1.17$$

For the reciprocal lattice vectors given in terms of the reciprocal lattice vectors $\boldsymbol{k} = k_1.\boldsymbol{k_1} + k_2.\boldsymbol{k_2}$ we can write E_2 as

$$E_2(k_1, k_2) = \varepsilon_{2p} - \gamma_0{}^2[f_{12}(k_1, k_2)] \quad 2.1.18$$

Where

$$f_{12}(k_1, k_2) = 3 + u(k_1, k_2),$$
$$u(k_1, k_2) = 2cos(2\pi k_1) + 2cos(2\pi k_2) + 2cos(2\pi(k_1 - k_2)) \quad 2.1.19$$

After some algebra we finally obtain the eigenvalues in the 1st nearest neighbor approximation that is used to generate the electronic band structure of graphene in Figure 2.1-2.

$$E(k_1,k_2)^{\pm} = \frac{\varepsilon_{2p} \pm \gamma_0\sqrt{f_{12}(k_1,k_2)}}{1 \pm s_0\sqrt{f_{12}(k_1,k_2)}} \qquad 2.1.20$$

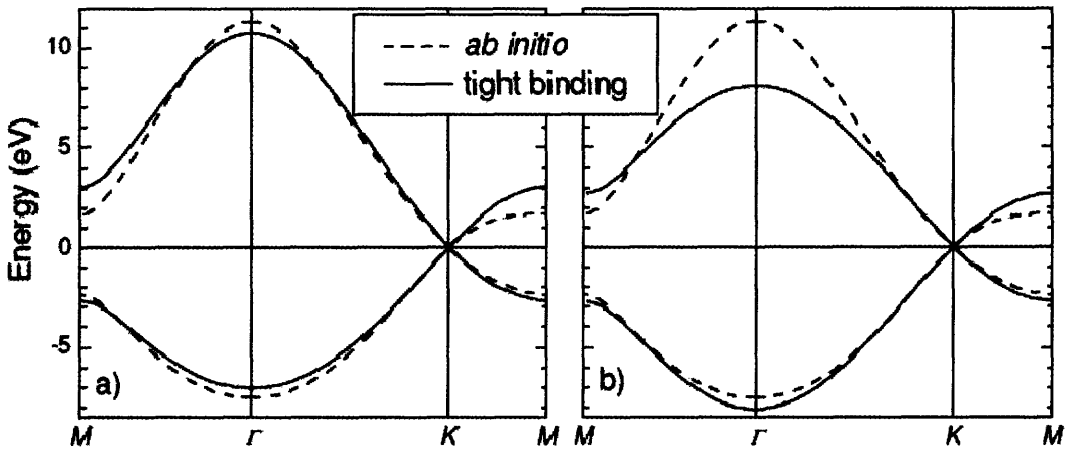

Figure 2.1-2 Nearest-neighbors tight-binding band structure of graphene. (a) Full lines show the best fit of the π bands with a finite overlap ($\gamma_0 = -2.84eV, s_0 = 0.07$). (b) Overlap s_0 set to zero. $\gamma_0 = -2.7eV$. The parameters were obtained by a least square fit to the ab-initio results close to the *K* point. The ab-initio band structure is shown by dashed lines. From Ref. (8).

2.1.2 3rd nearest neighbor approximation

Judging from the ab-initio tight-binding results (See Figure 2.1-2), an empirical calculation with third-nearest neighbor interaction should give a better description of the graphene band structure than the nearest neighbor model. In the Hamiltonian matrix and overlap elements we now have to further sum over the second neighbors A_{2i} $(i = 1,2 \ldots 6)$ and the third neighbors B_{3i} $(i = 1,2,3)$ (See Figure

2.1-1). Here we will simply give the results of the tedious calculation based on Ref. (9). We find for H_{AA} and H_{AB}

$$H_{AA} = \varepsilon_{2p} + \gamma_1 u(\boldsymbol{k}) \tag{2.1.21}$$

and

$$H_{AB} = \gamma_0(1 + e^{i\boldsymbol{k}.\mathbf{a}_1} + e^{i\boldsymbol{k}.\mathbf{a}_2})e^{-\frac{1}{3}i\boldsymbol{k}.(\mathbf{a}_1+\mathbf{a}_2)} + \gamma_2(1 + e^{-2i\boldsymbol{k}.\mathbf{a}_1} + e^{-2i\boldsymbol{k}.\mathbf{a}_2})e^{\frac{2}{3}i\boldsymbol{k}.(\mathbf{a}_1+\mathbf{a}_2)} \tag{2.1.22}$$

Where $\gamma_1$and γ_2 are the interaction energies for second and third neighbors, respectively. For S_{AA} and S_{AB} similar expression with s_1 and s_2 are obtained. In units of reciprocal lattice vectors, the E_i's relevant for Eq. (2.1.7) are given by

$$E_0 = (\varepsilon_{2p} + \gamma_1 u(k_1, k_2))[1 + s_1 u(k_1, k_2)] \tag{2.1.23}$$

$$E_1 = 2s_0\gamma_0 f_{12}(k_1, k_2) + (s_0\gamma_2 + s_2\gamma_0)g_{12}(k_1, k_2) + 2s_2\gamma_2 f_{12}(2k_1, 2k_2) \tag{2.1.24}$$

$$E_2 = (\varepsilon_{2p} + \gamma_1 u(k_1, k_2))^2 - {\gamma_0}^2 f_{12}(k_1, k_2) - \gamma_0\gamma_2 g_{12}(k_1, k_2) - {\gamma_2}^2 f_{12}(2k_1, 2k_2) \tag{2.1.25}$$

$$E_3 = (1 + s_1 u(k_1, k_2))^2 - {s_0}^2 f_{12}(k_1, k_2) - s_0 s_2 g_{12}(k_1, k_2) - {s_2}^2 f_{12}(2k_1, 2k_2) \quad 2.1.26$$

Where

$$g_{12}(k_1, k_2) = 2\, u(k_1, k_2) + u(2k_1 - k_2, k_1 - 2k_2) \quad 2.1.27$$

2.1.3 Extension of tight binding results to the phonon dispersion

We expect the Hamiltonian for ionic motion H_{ion} and the associated Hamiltonian for electron-phonon interaction H_{e-ion} (See Ref. (10)) to possess the same symmetry as that for the Hamiltonian H_e, for the electrons with the atoms cores fixed in position. This means that our tight binding result found in Eq. (2.1.7) may be used identically for generating the phonon dispersion. Indeed, all vibrational modes can be labeled just like electronic states based on their space group symmetry.

2.2 Perturbation theory

Sections 2.2.1, 2.2.2 and 2.2.2 closely follow the treatment found in Ref. (11).

2.2.1 The interaction representation

Consider a Hamiltonian H of a system that can be decomposed into the following components

$$H = H_0 + V \qquad 2.2.1$$

where the unperturbed Hamiltonian, H_0 is assumed to be time-independent. The perturbational coupling may or may not depend on time. The transition from the Schrodinger Representation to the interaction representation is achieved by applying a unitary transformation of the form

$$T(t) = e^{iH_0(t-t_0)/\hbar} \qquad 2.2.2$$

to the vectors $|\psi(t)>$ and operators A of the Schrodinger representation. t_0 is taken to be the origin of time. Thus, we get in the new representation

$$|\tilde{\psi}(t)> = e^{iH_0 t/\hbar}\,|\psi(t)> \qquad 2.2.3$$

$$\tilde{A}(t) = e^{iH_0 t/\hbar} A\, e^{-iH_0 t/\hbar} \qquad 2.2.4$$

As a result of the above transformations we find that $|\tilde{\psi}(t)>$ evolves only as a result of of the presence of perturbational coupling V . We can see this by applying the operator $i\hbar\frac{d}{dt}$ to Eq. (2.2.3) and using the Schrodinger Equation as follows

$$i\hbar\frac{d}{dt}|\tilde{\psi}(t)> = -H_0|\tilde{\psi}(t)> + e^{\frac{iH_0 t}{\hbar}}(H_0 + V)\,|\psi(t)> \qquad 2.2.5$$

$$= \tilde{V}(t)\,|\tilde{\psi}(t)> \qquad 2.2.6$$

Where $\tilde{V}(t) = e^{iH_0 t/\hbar} V\, e^{-iH_0 t/\hbar}$. Clearly from Eq. (2.2.6) we see that the vector $|\tilde{\psi}(t)>$ evolves only during the collision and not prior or after it.

In order to obtain the perturbative expansion of transition amplitudes we can write the following

$$|\psi(t_f)> = U(t_f, t_i)|\psi(t_i)> \qquad 2.2.7$$

Where $U(t_f, t_i)$ is the evolution operator. Performing the linear transformation of Eq. (2.2.3) on Eq. (2.2.7) above we get:

$$|\tilde{\psi}(t_f)> = \tilde{U}(t_f, t_i)|\tilde{\psi}(t_i)> \qquad 2.2.8$$

The evolution operator $U(t_f, t_i)$ satisfies

$$U(t_i, t_i) = 1 \qquad 2.2.9$$

Taking into account that the Schrodinger Equation, Eq. (2.2.7) is equivalent to the integral equation

$$U(t_f, t_i) = U_0(t_f, t_i) + \frac{1}{i\hbar}\int_{t_i}^{t_f} dt\, U_0(t_f, t) V\, U(t, t_i) \qquad 2.2.10$$

Where $U_0(t_f, t_i) = e^{\frac{-iH_0(t_f - t_i)}{\hbar}}$. By successive iterations, Eq. (2.2.10) thus leads to the perturbative expansion of the evolution operator

$$U(t_f, t_i) = U_0(t_f, t_i) + \sum_{n=1}^{\infty} U^{(n)}(t_f, t_i) \qquad 2.2.11$$

Where

$$U^{(n)}(t_f, t_i)$$

$$= \frac{1}{i\hbar}\int_{t_f \geq \tau_n \ldots \tau_2 \geq \tau_1 \geq t_i} d\tau_n \ldots d\tau_2 d\tau_1\, e^{-iH_0(t_f - \tau_n)/\hbar} V \ldots V e^{\frac{iH_0(\tau_2 - \tau_1)}{\hbar}} V e^{-iH_0(\tau_1 - t_i)/}$$

This then leads to

$$\tilde{U}(t_f, t_i) = 1 + \sum_{n=1}^{\infty} \tilde{U}^{(n)}(t_f, t_i) \qquad 2.2.13$$

Where

$$\tilde{U}^{(n)}(t_f, t_i)$$

$$= (\frac{1}{i\hbar})^n \int_{t_f \geq \tau_n \ldots \tau_2 \geq \tau_1 \geq t_i} d\tau_n \ldots d\tau_2 d\tau_1 \tilde{V}(\tau_n) \ldots \tilde{V}(\tau_2)\tilde{V}(\tau_1) \qquad 2.2.14$$

Let ξ_{fi} be the matrix element of $\tilde{U}(t_f, t_i)$ between the eigenstates φ_f and φ_i of the Hamiltonian H_0

$$\xi_{fi} = < \varphi_f | \tilde{U}(t_f, t_i) | \varphi_i > \qquad 2.2.15$$

which yields

$$\xi_{fi} = \delta_{fi} + \sum_{n=1}^{\infty} \xi_{fi}{}^{(n)} \qquad 2.2.16$$

Where

$$\xi_{fi}{}^{(n)} = < \varphi_f | \tilde{U}^{(n)}(t_f, t_i) | \varphi_i > \qquad 2.2.17$$

2.2.2 First order transition amplitude

We can now proceed to calculate the first order of this perturbative expansion for the transition amplitude ξ_{fi}. Using Eq. (2.2.17) and (2.2.14) we get

$$\xi_{fi}{}^{(1)} = \frac{1}{i\hbar}\int_{t_i}^{t_f} d\tau_1 < \varphi_f|V|\varphi_i > e^{i\tau_1(E_f-E_i)/\hbar} \qquad 2.2.18$$

If we make the assumption that V is independent of time and take the limits on the integration to be $t_i = -\frac{T}{2}, t_f = \frac{T}{2}$ we get

$$\xi_{fi}{}^{(n)} = -2\pi i < \varphi_f|V|\varphi_i > \delta^{(T)}(E_f - E_i) \qquad 2.2.19$$

Where $\delta^{(T)}(E_f - E_i) = \frac{Sin(E_f-E_i)T/2\hbar}{\pi(E_f-E_i)}$ which tends to $\delta(E_f - E_i)$ as $T \to \infty$. Hence this function is an approximate delta function expressing the conservation of energy with an uncertainty $\hbar/T$ due to the finite duration of the interaction.

2.2.3 Second order transition amplitude

For the second order Eqs. (2.2.17) and (2.2.14) give

$$\xi_{fi}^{(2)}(t_f, t_i) = \frac{1}{i\hbar}^2 \int_{\frac{T}{2}\geq\tau_2\geq\tau_1\geq -T/2} d\tau_2 d\tau_1 \sum_k < \varphi_f|V|\varphi_k \\ >< \varphi_k|V|\varphi_i > e^{i\tau_2(E_f-E_k)/\hbar} e^{i\tau_1(E_k-E_i)/\hbar} \qquad 2.2.20$$

Again assuming V is time-independent and calculating the integral using the method of residues and carrying algebraic manipulations we get:

$$\xi_{fi}^{(n)} \\ = -2\pi i[\lim_{\eta\to 0_+} \sum_k \frac{< \varphi_f|V|\varphi_k >< \varphi_k|V|\varphi_i >}{E_i - E_k + i\eta}]\delta^{(T)}(E_f \qquad 2.2.21 \\ - E_i)$$

2.2.4 Feynman diagrams

In order to enumerate all the terms for the Second Order Transition amplitude shown in Eq. (2.2.21) we make use of Feynman Diagrams. Here we will show what they are and how to use them without discussing them in detail following Ref. (10).

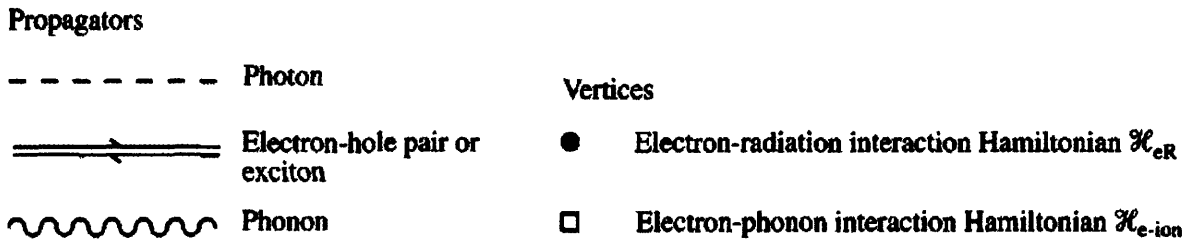

Figure 2.2-1: Symbols used in drawing Feynman diagrams to represent Raman scattering. From Ref. (10).

The rules for drawing Feynman diagrams are:

- Excitations such as photon, phonons and electron-hole pairs in Raman scattering are represented by propagators as shown in Figure 2.2-1. These are labeled with their corresponding wavevectors, frequencies, and polarizations etc.

- The interaction between two (or more) excitations is represented by an intersection of propagators and is known as a vertex. These are rendered as filled circles or empty squares in Figure 2.2-1.

- The arrows on the propagators indicate creation and annihilation of their corresponding excitations. Arrows pointing away from a vertex indicate creation whilst those pointing towards a vertex indicate annihilation.

- Chronologically, Feynman diagrams are read from left to right.

- Different time orders may be generated by simply permuting the order of the vertexes in the diagram.

Figure 2.2-2: Feynman Diagram for a Process that contributes to One-Phonon Raman Scattering. From Ref. (10).

We shall illustrate the application of Feynman diagrams by using them to represent the Raman scattering by phonons following Ref. (12) (13). The diagram for the simplest Raman process is shown in Figure 2.2-2.

Once all the possible Feynman diagrams have been drawn, these are translated into the required perturbative expansions of the scattering probability. We make use of Fermi's golden rule to derive the the probability for scattering a system from the initial state $|i>$ to the $|f>$ state.

Consider the diagram in Figure 2.2-2. The first vertex introduces a term of the form

$$\sum_{n} \frac{< n|\mathcal{H}_{eR}(\omega_i)|i >}{[\hbar\omega_i - (E_n - E_i)]} \qquad 2.2.22$$

into the scattering probability. Here $|i>$ is taken to be the initial state and E_i is its energy. $|n>$ denotes any intermediate electronic state with energy E_n. The sign of $\hbar\omega_i$ in the energy denominator depends on whether the quantum of energy $\hbar\omega_i$ was absorbed (+ sign) or emitted (-sign). The summation in Eq. (2.2.22) is taken over all intermediate states $|n>$. When there is a second vertex, as in Figure 2.2-2., Eq. (2.2.22) is multiplied by another similar term to become

$$\sum_{n,n'} \frac{< n'|\mathcal{H}_{e-ion}(\omega_0)|n >< n|\mathcal{H}_{eR}(\omega_i)|i >}{[\hbar\omega_i - (E_n - E_i)][\hbar\omega_i - (E_n - E_i) - \hbar\omega_0 - (E_{n'} - E_n)]} \qquad 2.2.23$$

Where $|n'>$ is another intermediate state. The sign of $\hbar\omega_0$ in the denominator is negative now because a quasiparticle (a phonon in this case) is created. Each

vertex adds a matrix element of the interaction Hamiltonian to the numerator and an energy term to the denominator. Eq. (2.2.23) can be further simplified to read

$$\sum_{n,n'} \frac{< n'|\mathcal{H}_{e-ion}(\omega_0)|n >< n|\mathcal{H}_{eR}(\omega_i)|i >}{[\hbar\omega_i - (E_n - E_i)][\hbar\omega_i - \hbar\omega_0 - (E_{n'} - E_i)]} \qquad 2.2.24$$

These terms are included till all the vertices are exhausted. Although in principle, there ought to be the same number of energy terms as the number of vertices in the diagram. However, the last vertex represents the overall energy conservation condition and is converted to a delta function.

Therefore for the diagram considered in Figure 2.2-2 we get the so called *Raman matrix element,* $K_{2f,10}$ (14), as

$$K_{2f,10} = \sum_{n,n'} \frac{< n'|\mathcal{H}_{e-ion}(\omega_0)|n >< n|\mathcal{H}_{eR}(\omega_i)|i >}{[\hbar\omega_i - (E_n - E_i)][\hbar\omega_i - \hbar\omega_0 - (E_{n'} - E_i)]} \qquad 2.2.25$$

Different time orders contribute terms that are simply added to the expression within the summation sign to suitably modify $K_{2f,10}$.

2.3 The double resonant process

Double Resonant Raman scattering -where two of the intermediate electronic states must be real, plays an important role in interpreting the Raman spectra of graphene, graphite and carbon nanotubes thereby providing a wealth of information about their electro-vibrational states. In such carbon based materials and therefore particularly in graphene it is the dominant process and has been successful in explaining various features of the Raman Spectra of these materials such as their D mode and its hitherto curious dependence on the excitation energy (4), (14), (15), (5). In graphite, carbon nanotubes, and other forms of sp^2-bonded carbon, several defect-induced and second-order double-resonant modes are observed, of which the most prominent one is the so-called D-mode at ~ 1380 cm^{-1}. The first part of this section aims to describe the double-resonant Raman Scattering in graphene in a 1-dimensional setting and the latter part extends this to two-dimensions based on our research.

2.3.1 One dimensional calculation

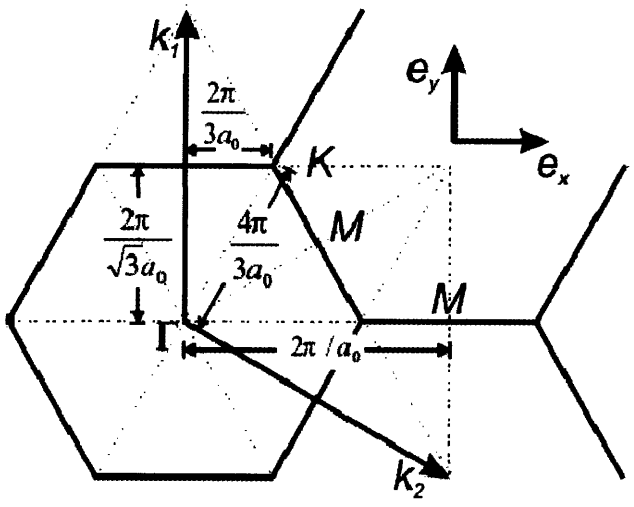

Figure 2.3-1: Brillouin zone of graphene with the high-symmetry points Γ, *K*, *M*.

Consider the *K* point in the Brillouin zone of graphene (See Figure 2.3-1 and Figure 2.3-2). The solid line from *a* to *b* in Figure 2.3-2 shows only the resonant contribution involving a phonon that scatters the electron from the electronic eigenstate *a* to another electronic eigenstate *b*. Phonon emission conserves quasi-momentum and the change in the *k* values of electronic eigenstates *a* and *b* is compensated via the *q* of the phonon. Likewise for energy conservation, where the energy difference between the two eigenstates is again compensated by the phonon.

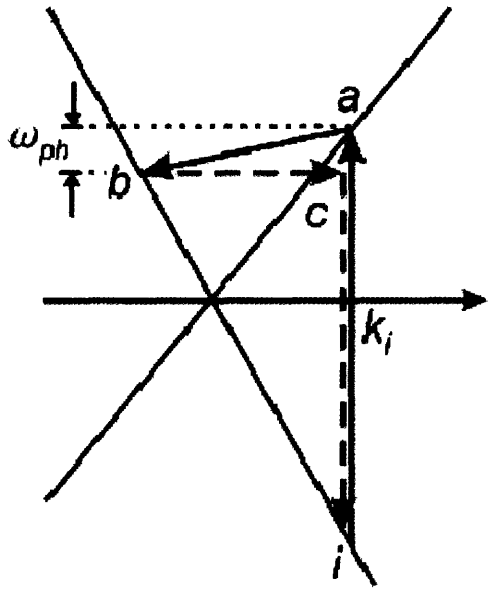

Figure 2.3-2: A Schematic of the Double resonance process in graphene about the *K* point. From Ref. (8).

A continuously varying band gap implies that the incoming photon is always resonant. A second resonant transition is made from electronic eigenstates $a \rightarrow b$ with the emission of a phonon. Such a process is depicted in Figure 2.3-2 and adds a second resonance to the Raman process. The third transition $b \rightarrow c$ occurs due to elastic defect or surface scattering which cannot be resonant as the electronic eigenstate is not a real state. Once the electronic eigenstate c is reached the electron simply recombines with a hole and we get back the original electronic eigenstate i conserving quasi-momentum. The second possibility, inelastic scattering with another phonon, leads to a Raman signal at twice the phonon energy and does not require a defect to conserve momentum.

Application of perturbation theory to the aforementioned process leads to the so-called *Raman matrix element* $K_{2f,10}$ of the form (16) (where we have followed the nomenclature from Ref. (5))

$$K_{2f,10} = \sum_{a,b,c} \frac{M_{eR,\rho} M_{e-defect} M_{ep} M_{eR,\sigma}}{(E_1 - E_{ai}^e - i\gamma)(E_1 - \hbar\omega_{ph} - E_{bi}^e - i\gamma)(E_1 - \hbar\omega_{ph} - E_{ci}^e - i\gamma)} \quad 2.$$

We have abbreviated the matrix elements in the numerator by M_i. Specifically, $M_{e-defect}$ refers to the elastic interaction of the defect and the scattered electron. Not much is known about this interaction and the assumption that it is elastic and symmetry conserving for the scattered carrier. As mentioned in section 2.2.4, we have to include all the possible time orders i.e., phonon scattering followed by defect scattering and vice-versa, and include the hole instead of the electron as well. The Feynman diagrams corresponding to the 1st and 2nd time order of the double resonant process in graphene are given in Figure 2.3-3 and Figure 2.3-4 respectively.

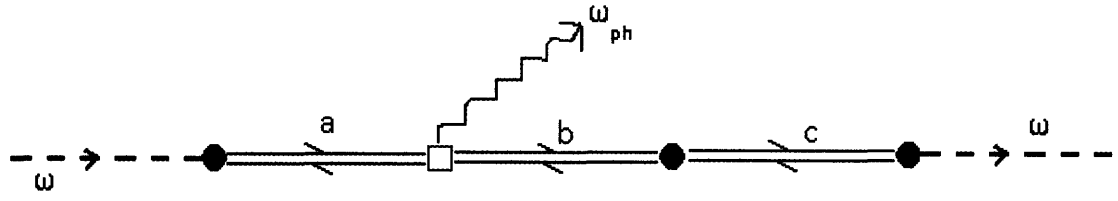

Figure 2.3-3: First time order (phonon first, defect second) Feynman diagram for double resonant process in graphene.

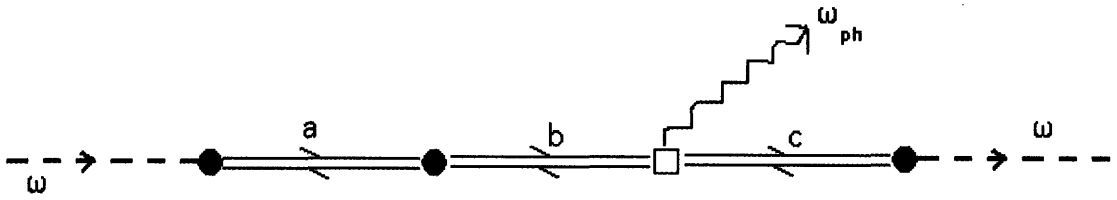

Figure 2.3-4: Second time order (defect first, phonon second) Feynman diagram for double resonant process in graphene.

A change in incoming photon energy (say $i' \rightarrow a$) leads to an excited electron with a different momentum. In order to fulfill the second resonant transition a phonon with different quasi-momentum is required and in particular, a larger incoming photon energy requires a larger phonon wave vector, that depending on the phonon dispersion involves a higher or lower phonon energy. Therefore, scanning the incident photon energy is tantamount to scanning the phonon energy in q-space.

We now show the analytical calculation, attributed to Reich and Thomsen from Ref. (4) for the Raman Cross-section of the D mode in the approximation of linear bands in one-dimension.

At the K point, the electronic bands are approximately linear for the transition energies in the visible range of light and cross the Fermi-level. In Figure 2.3-5 both the possibilities for scattering between the same electronic bands are shown in where v_1, v_2 are the Fermi velocities (or slopes of the energy bands) and k and q .

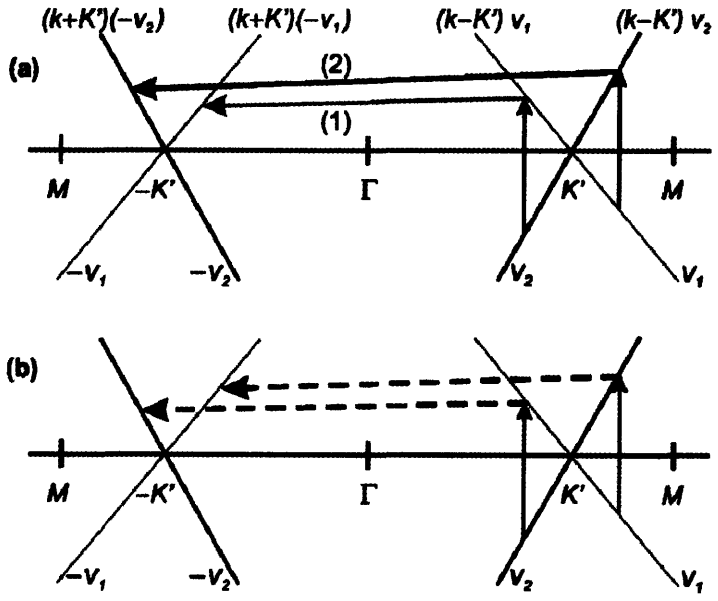

Figure 2.3-5: Linear bands of graphene with (a) D mode scattering taking place across the Γ point within the same electronic band and, (b) Scattering across the Γ point between two almost parallel bands does not contribute to the double resonant signal due to destructive interference. From Ref. (5).

For the linear bands in Figure 2.3-2, we can calculate the expression given by Eq. (2.3.1), explicitly noting that for a semi-metal like graphite the electronic energies can be expressed as a function of k and Fermi-velocities as: $E_{ai}^{e} = \frac{|k|}{v_2 - v_1}$, $E_{bi}^{e} = \mp q v_{1/2}$, $E_{ci}^{e} = \frac{|k|}{v_2 - v_1}$ with $v_1 < 0$ and $v_2 > 0$ being the Fermi velocities. In one dimension converting to an integral over k:

$$K_{2f,10} = \frac{M_{eR,\rho} M_{e-defect} M_{ep} M_{eR,\sigma}}{(v_1 - v_2)^3 \left(\kappa_2 - q\frac{v_2}{v_2 - v_1}\right)\left(\kappa_2 + q\frac{v_1}{v_2 - v_1}\right)} \int_0^{\infty} \frac{dk}{(\kappa_1 - k)(\kappa_2 - k)} \quad 2.$$

Where $\kappa_1 = \frac{E_1 - i\gamma}{v_2 - v_1}$ and $\kappa_2 = \frac{E_1 - \hbar\omega_{ph} - i\gamma}{v_2 - v_1}$. As is evident from the above expression, we have taken the matrix elements to be constant. Besides the interaction containing the defect, all other matrix elements can be calculated and will feature in our future work. The expression in Eq. (2.3.1) evaluates to:

$$K_{2f,10} = \frac{a M_{eR,\rho} M_{e-defect} M_{ep} M_{eR,\sigma}}{\left(\kappa_2 - q\frac{v_2}{v_2 - v_1}\right)\left(\kappa_2 + q\frac{v_1}{v_2 - v_1}\right)} \quad 2.3.3$$

Where $a = Log(\frac{\kappa_2}{\kappa_1})\frac{(2\kappa_2 - q)}{(v_2 - v_1)^2 \hbar\omega_{ph}}$ is a slowly varying function of q. As is indicated by the expression, the strongest resonant enhancement is given when both terms in the denominator simultaneously approach zero.

Figure 2.3-6 plots $|K_{2f,10}|^2$ for graphene for two incoming photon energies. For each photon energy there are <u>two</u> maxima whose separation depends on the Fermi velocities that are adapted from the band structure of graphene.

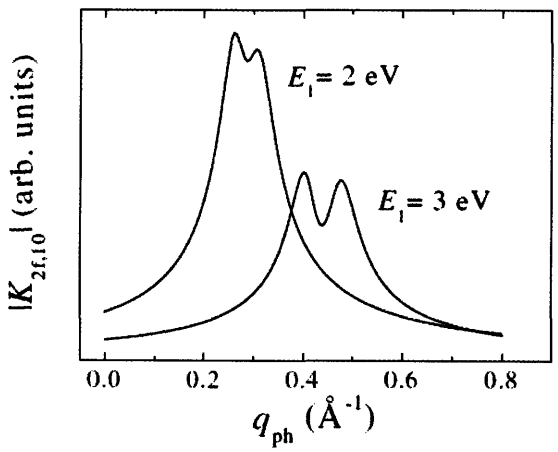

Figure 2.3-6: The absolute magnitude of the Raman matrix element $|K_{2f,10}|^2$ for two incident photon energies based on the one dimensional model. From Ref. (4).

2.3.2 Two dimensional calculation

We now consider the same double-resonant Raman process in a more realistic two-dimensional setting for a single sheet of graphene. Under the tight binding approximation, the electronic band-gap of graphene was obtained from Eq. (2.1.20) as

$$E_g(k_1,k_2) = \gamma_0\sqrt{f_{12}(k_1,k_2)}\left[\frac{1}{1-s_0\sqrt{f_{12}(k_1,k_2)}} - \frac{1}{1+s_0\sqrt{f_{12}(k_1,k_2)}}\right] \qquad 2.3.4$$

Where $\gamma_0 = 2.84\ eV$, $s_0 = 0.07$ and $f_{12}(k_1,k_2) = 3 + u(k_1,k_2)$, $u(k_1,k_2) = 2cos(2\pi k_1) + 2cos(2\pi k_2) + 2cos(2\pi(k_1 - k_2))$.

Figure 2.3-7 shows the smallest irreducible portion (region enclosed by parallelogram) of the graphene Brillouin zone on which we can render the electronic band-gap as a contour plot.

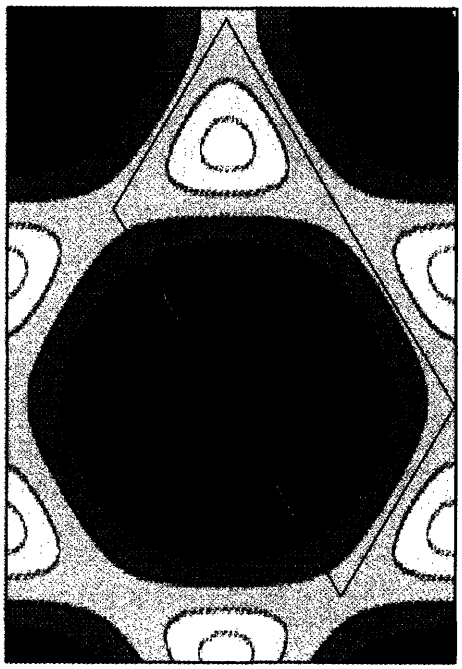

Figure 2.3-7: Band-gap of graphene superimposed on the smallest irreducible portion of its Brillouin zone (region enclosed by parallelogram).

For the case of 1st nearest neighbor interaction, the phonon dispersion of graphene was fitted to experimental data for it's TO branch (17), (18), (19), (20), (21), (22) (See also section 2.4: Symmetry and selection rules) as shown in Figure 2.3-8 and using the tight binding expression from Eq. (2.1.20) derived earlier.

$$\omega_{ph}(q_1, q_2) = 8065.5\left[\frac{0.155+0.07833\sqrt{f_{12}(k_1,k_2)}}{1+0.333\sqrt{f_{12}(k_1,k_2)}}\right](cm^{-1}) \qquad 2.3.5$$

which gives a very similar contour plot and irreducible Brillouin zone as the one given by Figure 2.3-7.

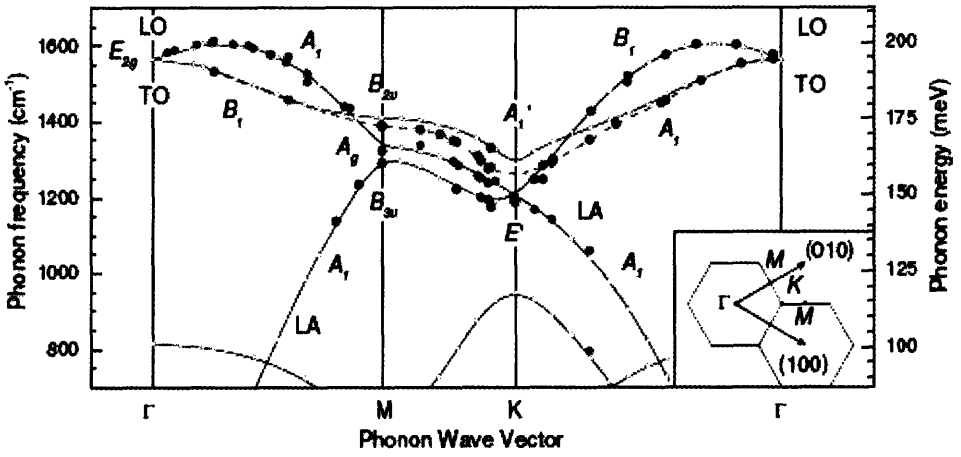

Figure 2.3-8: Phonon dispersion of graphite. From Ref. (22).

In order to calculate the *Raman matrix element* $K_{2f,10}$ we implemented a *parallelized* numerical code, details of which shall be given in sections 2.5 and 5. We generated results parameterized by incoming laser energy, damping coefficient terms and band-gap structure (in order to simulate multiple graphene layers). A sample plot of $|K_{2f,10}|^2$ v/s phonon energy ω_{ph} (cm^{-1}) is shown in Figure 2.3-9.

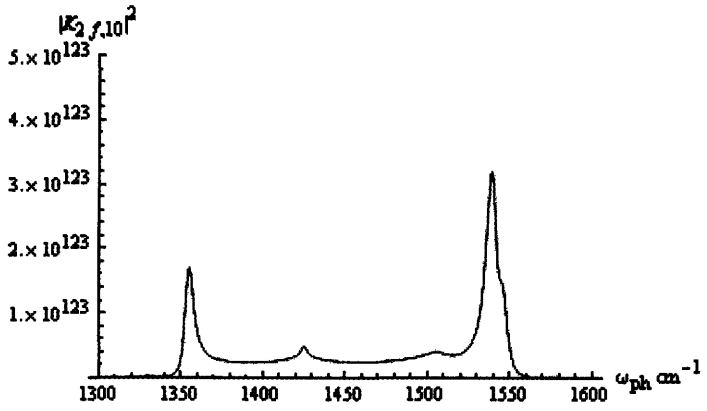

Figure 2.3-9: Plot of $|K_{2f,10}|^2$ v/s ω_{ph} (cm^{-1}) for incoming photon energy $E_1 = 2.00eV$

Figure 2.3-9 shows that a single D mode peak in is present nominally at 1380 cm^{-1} for the given experimental conditions and model band structure and phonon dispersion. Our results show that this peak shifts at a rate of 30-40 cm^{-1}/eV of incoming photon energy which is well in line with experimental results.

2.4 Symmetry and selection rules

This section aims to uncover those phonon branches that make the dominant contribution towards the Raman cross-section due to the double-resonant process.

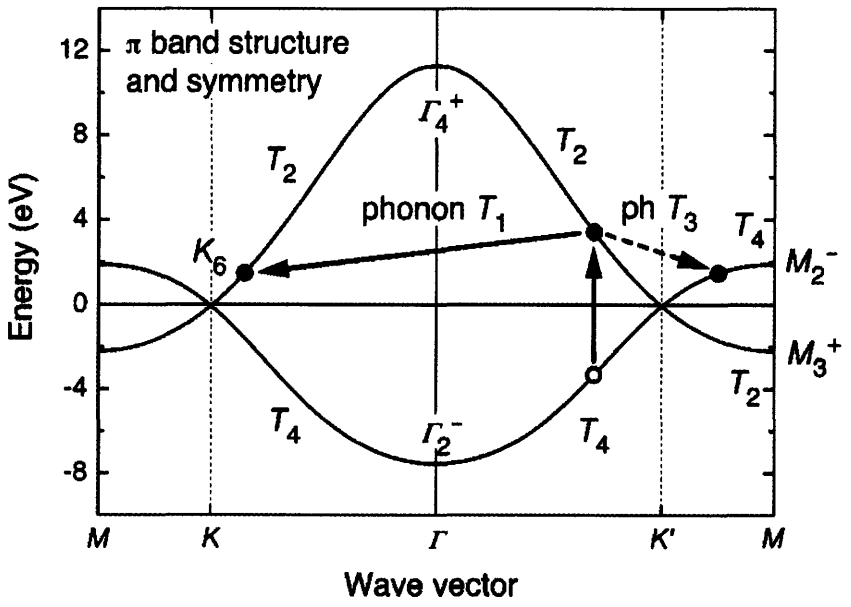

Figure 2.4-1: shows the 3rd nearest neighbor electronic π and π^* bands along $\Gamma - K - M$ for graphene based on the results shown in section 2.1. The symmetry representations are marked next to each branch. The solid arrows represents phonon scattering across the Γ point, and the dashed line phonon scattering across the K point. From Ref. (5).

Figure 2.4-1 shows the electronic band structure of graphene (based on the 3rd nearest neighbor tight binding model of section 2.1.2) between the high symmetry points $\Gamma - K - M$. The points excluding the points of high symmetry i.e, Γ, K, M

have a reduced symmetry group C_{2v}, as compared to the point group of graphene that has symmetry D_{6h}. For the branches $\Gamma - K$ and $\Gamma - K'$, the valence band possesses a symmetry T_4 and the conduction band a symmetry T_2. Whereas for the branches $K - M$ and $K' - M$, the situation is reversed such that the conduction band possesses symmetry T_4 and the valence band the symmetry T_2. For both the above cases, a photon with symmetry Γ_6^- is required for optical excitation. Subsequently, the phonon may scatter within the same band which is also known as scattering across the Γ point (See Figure 2.4-1) via the solid line , and therefore same symmetry ($T_2 \rightarrow T_2$, $T_4 \rightarrow T_4$) that consequently requires it to possess a totally symmetric representation, T_1. The other possibility being that that the phonon scatters across bands (scattering across the K point) with a different symmetry ($T_2 \rightarrow T_4$ or $T_4 \rightarrow T_2$) which require the phonon to possess the symmetry corresponding to the T_3 representation.

As for phonon scattering across the K point, due to the peculiar nature of the electronic bands in graphene, the third step of the double resonant process (elastic defect scattering) has a much higher likelihood of being a virtual state rather than a real state. This is due to the enhanced difference between the band energies compared to the case for scattering across the Γ point. Therefore, defect scattering subsequent to phonon scattering across the K point is much weaker than that

subsequent to the phonon scattering across the Γ point as it is much less likely to be resonant for all but the smallest incoming photon energies. All this means that we can safely neglect the contribution of the phonon branches possessing T_3 symmetry.

This leaves us to focus on only those phonon branches that possess the correct symmetry T_1 that contribute to the double resonant process.

Referring to Figure 2.3-8, we find that only the TO branch, which has a minimum symmetry T_1 throughout, makes the dominant contribution to the double resonant process. Although the LA branch possesses the correct symmetry between the high symmetry points it lacks the requisite symmetry at both the K and Γ points and hence its contribution may be safely precluded in our model.

In the above discussion we have tacitly made the assumption that the defect scattering takes place between states of same symmetry, which even if relaxed would result only in a diminished contribution via its corresponding matrix element. In any case, the resonant contributions of intermediate states (possessing a different symmetry) are much weaker than for real states therefore validating our assumption.

These predictions are borne out very well by the results of our calculations as the Raman spectra so obtained possesses a remarkably high fidelity with experimental results.

2.5 Computational requirements

2.5.1 Computational resources

Our simulations were carried out primarily on a dual Quad-Core Intel® x86 processor machine with 16 GB RAM, with all cores running simultaneously to parallelize our calculation.

2.5.2 Software

- Our code was written in Mathematica v.5.2 and we used the additional component Mathematica Parallel Toolkit v.1.0 to parallelize certain portions of our code.
- For graphing we used Mathematica v.5.2 and v.6.0 and Origin v.7.5

2.5.3 Computational complexity

- First, the expression $fu1$ and $fu2$ (See Mathematica code in section 5) representing each of the two time orders in the perturbational expression are summed separately over all the points (k_1, k_2) that comprise the irreducible portion of the Brillouin zone to generate $fu1$ and $fu2$ as a function of the phonon vectors (q_1, q_2) . We divided the Brillouin zone into 401*200 = 80200 distinct (k_1, k_2) points.
- Each of these expression $fu1$ and $fu2$ are evaluated for each (q_1, q_2). Again we used 401*200 = 80200 distinct (q_1, q_2) points.
- The complex valued expressions $fu1$ and $fu2$ obtained for each (q_1, q_2) were summed to finally obtain $K_{2f,10}(q_1, q_2)$
- In order to generate the Raman Spectra, i.e., $|K_{2f,10}|^2$ v/s ω_{ph} (cm^{-1}) we mapped $K_{2f,10}(q_1, q_2) \rightarrow K_{2f,10}(\omega_{ph})$ using the phonon dispersion $\omega_{ph}(q_1, q_2)$ (cm^{-1}). A smooth continuous curve for $|K_{2f,10}|^2$ v/s ω_{ph} (cm^{-1}) was obtained by summing a series of normalized *Gaussian's* multiplied by $K_{2f,10}(\omega_{ph})$. The complete code is given in section 5.

3 Raman spectra of graphene

3.1 Results of calculation with 1st nearest neighbor phonon dispersion

3.1.1 Electronic band structure used for calculation

The electronic band structure of graphene was obtained by fitting the expression obtained in Eq. (2.1.20) to the ab-initio electronic band structure obtained from an ab-initio tight binding code, Ref. (23) . We rewrite Eq. (2.1.20) here for convenience

$$E(k_1,k_2)^{\pm} = \frac{\varepsilon_{2p} \pm \gamma_0\sqrt{f_{12}(k_1,k_2)}}{1 \pm s_0\sqrt{f_{12}(k_1,k_2)}} \qquad 3.1.1$$

Where

$$
\begin{aligned}
f_{12}(k_1, k_2) &= 3 + u(k_1, k_2), \\
& \\
& u(k_1, k_2) \\
& = 2cos(2\pi k_1) + 2cos(2\pi k_2) \\
& + 2cos(2\pi(k_1 - k_2))
\end{aligned}
\qquad 3.1.2
$$

The fitting of Eq. (3.1.1) yielded the following values for the values of the constants

$$
\begin{aligned}
\varepsilon_{2p} &= 0 \\
\gamma_0 &= 2.84\, eV \\
s_0 &= 0.07
\end{aligned}
\qquad 3.1.3
$$

A plot of the valence and conduction bands for graphene based on Eq. (3.1.1) and the constants listed in Eq. (3.1.3) is given in Figure 3.1-1 and Figure 3.1-2 respectively.

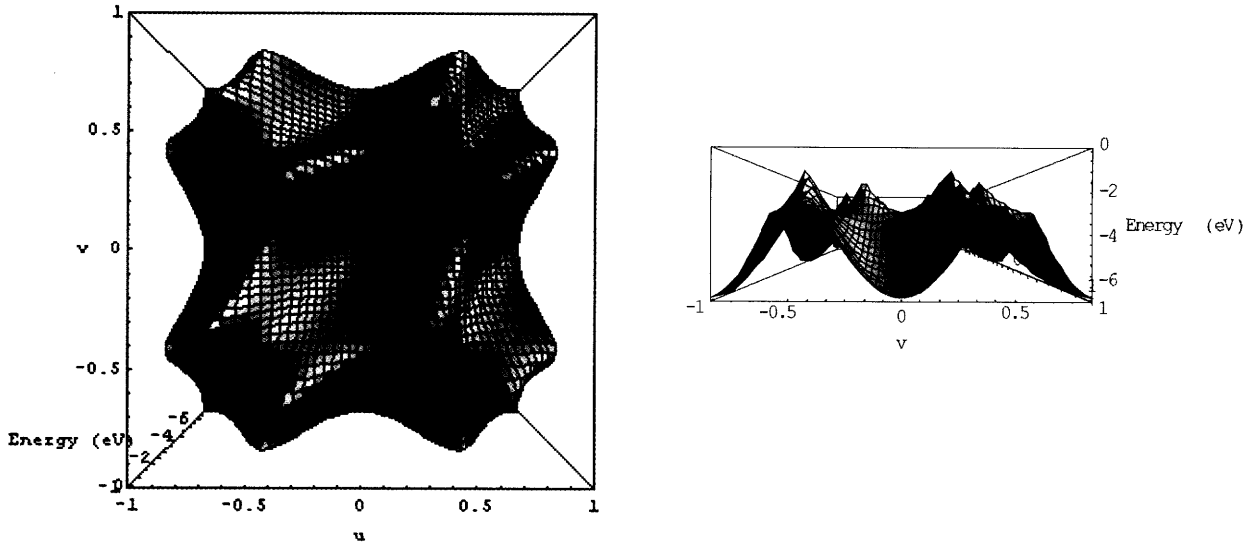

Figure 3.1-1: Different views of the valence band of graphene, (a) and (b)

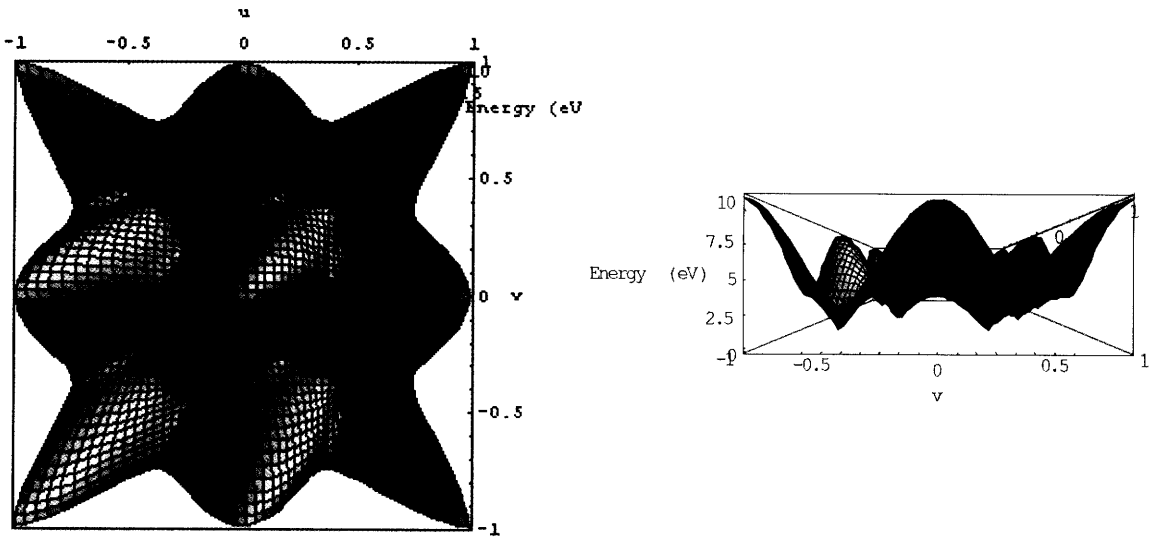

Figure 3.1-2: Different views of the conduction band of graphene, (a) and (b)

The following Figure 3.1-3 shows the valence and conduction bands together for easy viewing

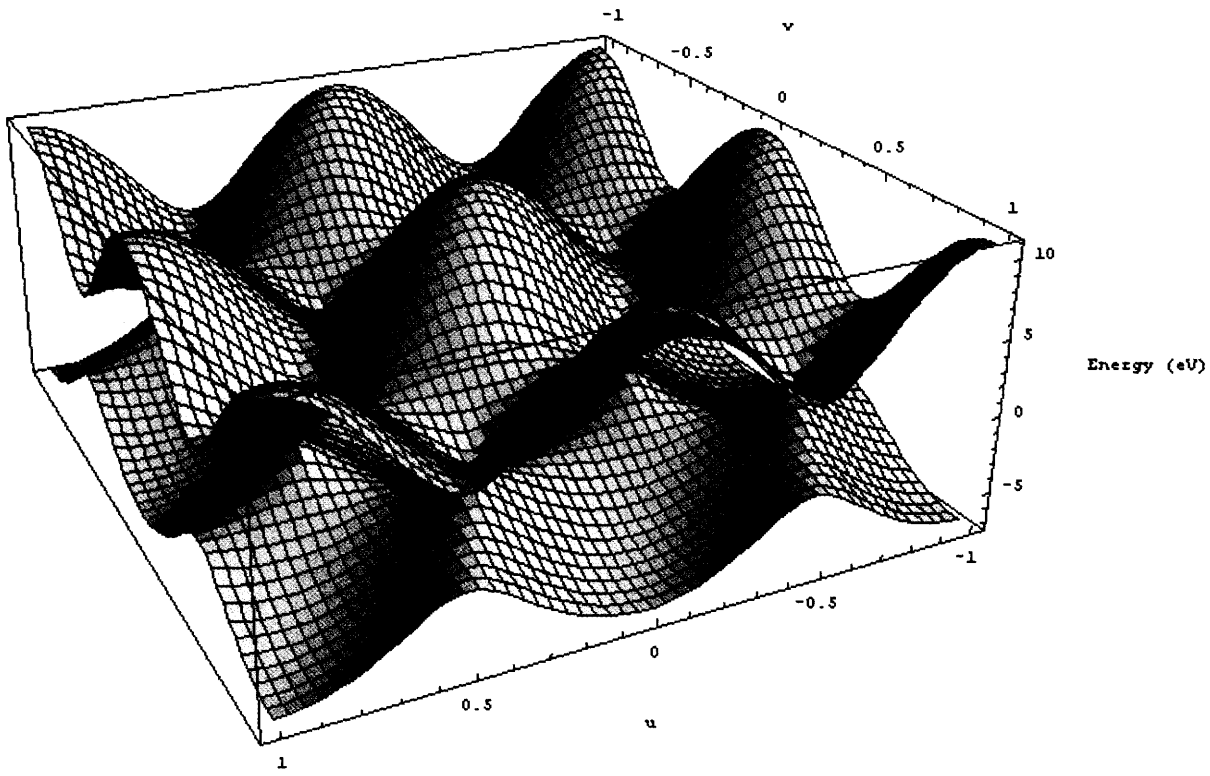

Figure 3.1-3: Valence and conduction bands in graphene.

Note the crossing of the bands at the *K* points or alternatively, that the band gap at the *K* points is zero.

3.1.2 Phonon dispersion used for calculation

The phonon dispersion used for our calculations is the same $E^{+}(q1, q2)$ as from Eq. (2.1.20) used to generate the electronic band structure of graphene with the assumption of the 1st nearest neighbor interaction (See section 2.1.3). The constants were fitted to inelastic X-ray scattering performed by Maultzsch et al from Ref. (22). The values of the constant obtained on fitting the date were obtained as:

$$\begin{aligned} \varepsilon_{2p} &= 0.155e \\ \gamma_0 &= -0.07833 * 8065.5\ cm^{-1} \\ s_0 &= 0.333 \end{aligned} \qquad 3.1.4$$

The plot of phonon energy in units of cm^{-1} is given in Figure 3.1-4 below

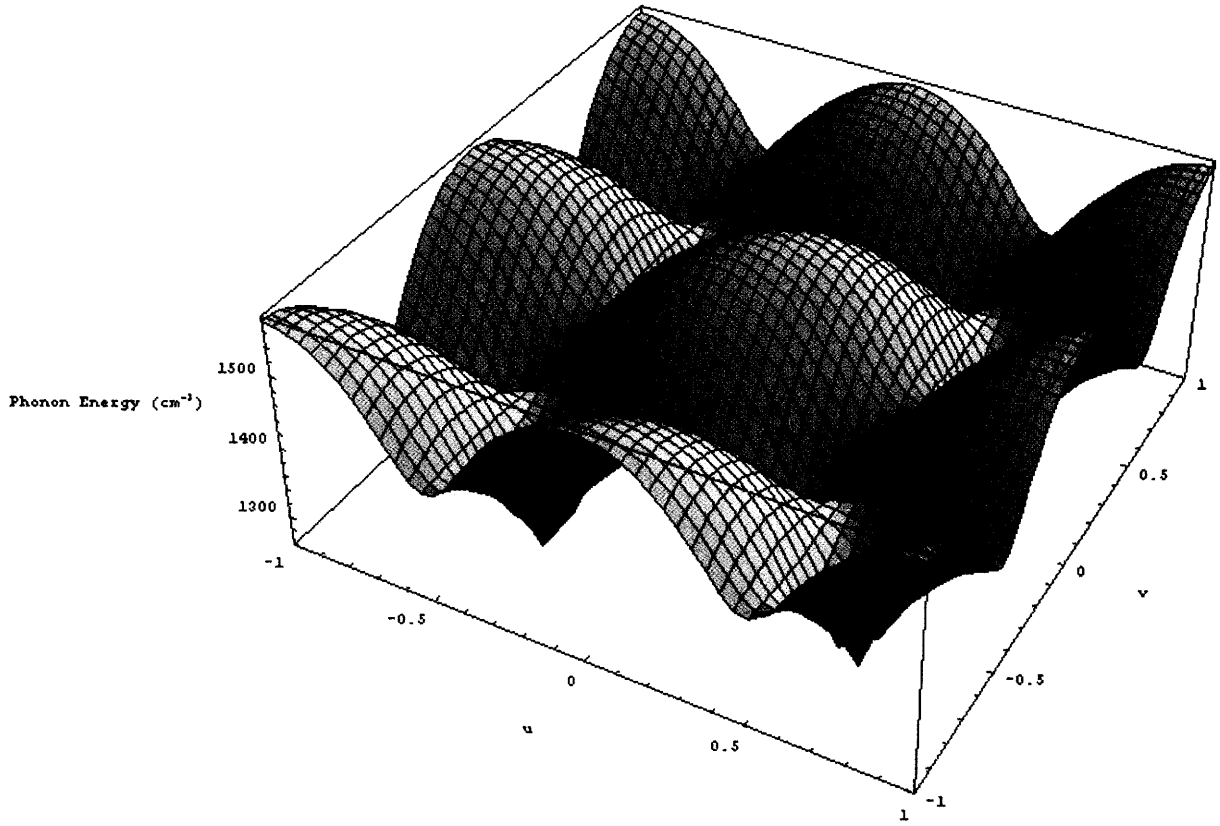

Figure 3.1-4: Phonon Dispersion of Graphene

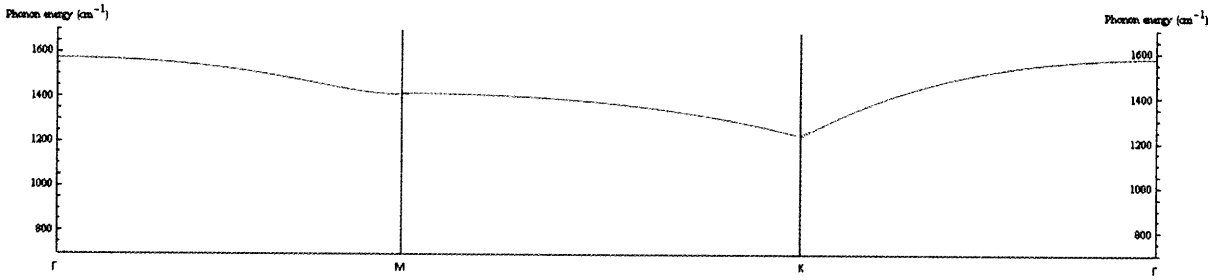

Figure 3.1-5: $\Gamma - K - M$ Phonon Dispersion of Graphene based on the 1st nearest neighbor interaction

3.1.3 Overlays of $|K_{2f,10}(q1, q2)|$ on the phonon dispersion $\omega_{ph}(q1, q2)$

The following overlays of $|K_{2f,10}(q1, q2)|$ over the phonon dispersion $\omega_{ph}(q1, q2)$ shall help us easily visualize the evolution of the highly resonant contributions (given by the *red* portions of the figure) with the change in excitation energy.

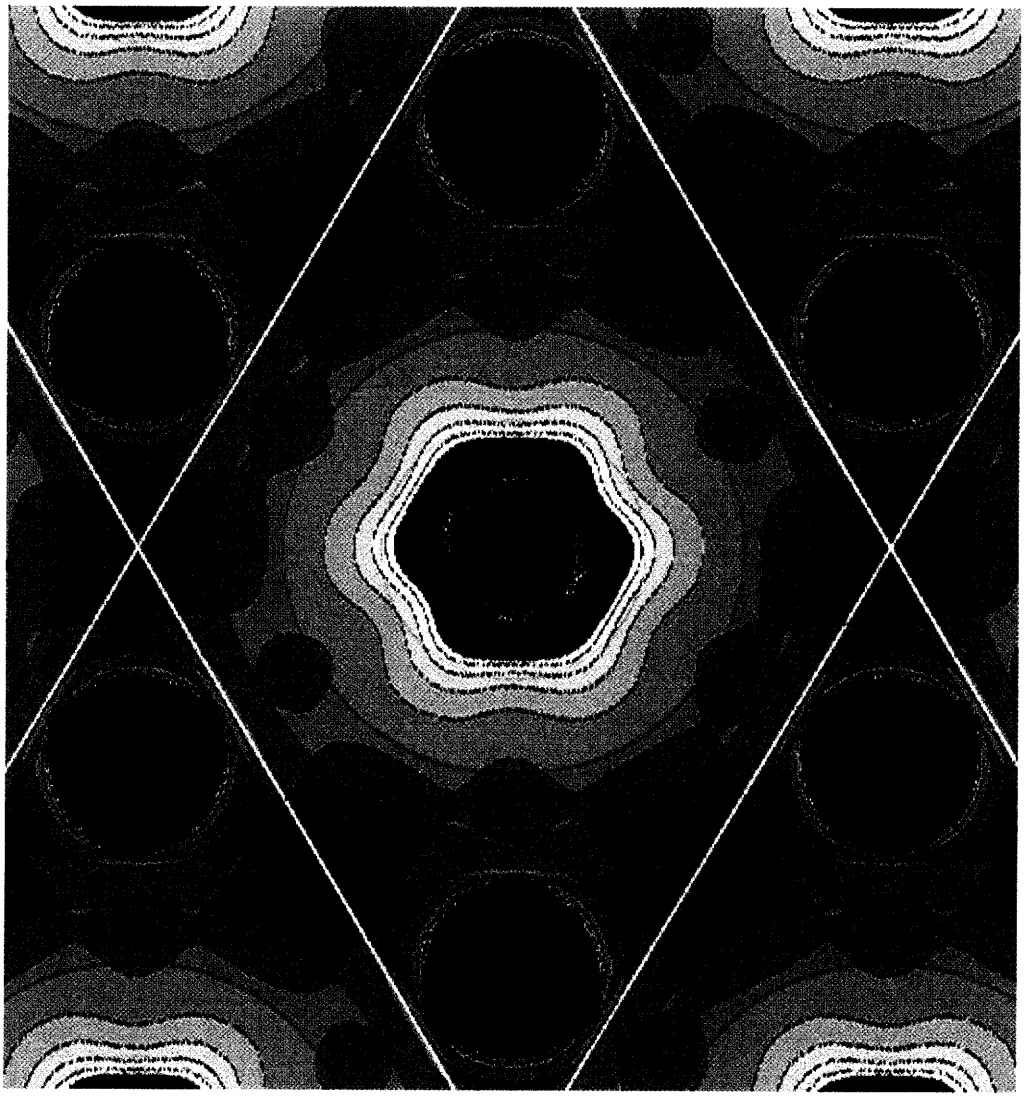

Figure 3.1-6: Overlay of $|K_{2f,10}(q1, q2)|$ for laser energy $2.00eV$ on the 1st nearest neighbor phonon dispersion. The resonant contributions are highlighted in red. (Ignore the solid lines in white)

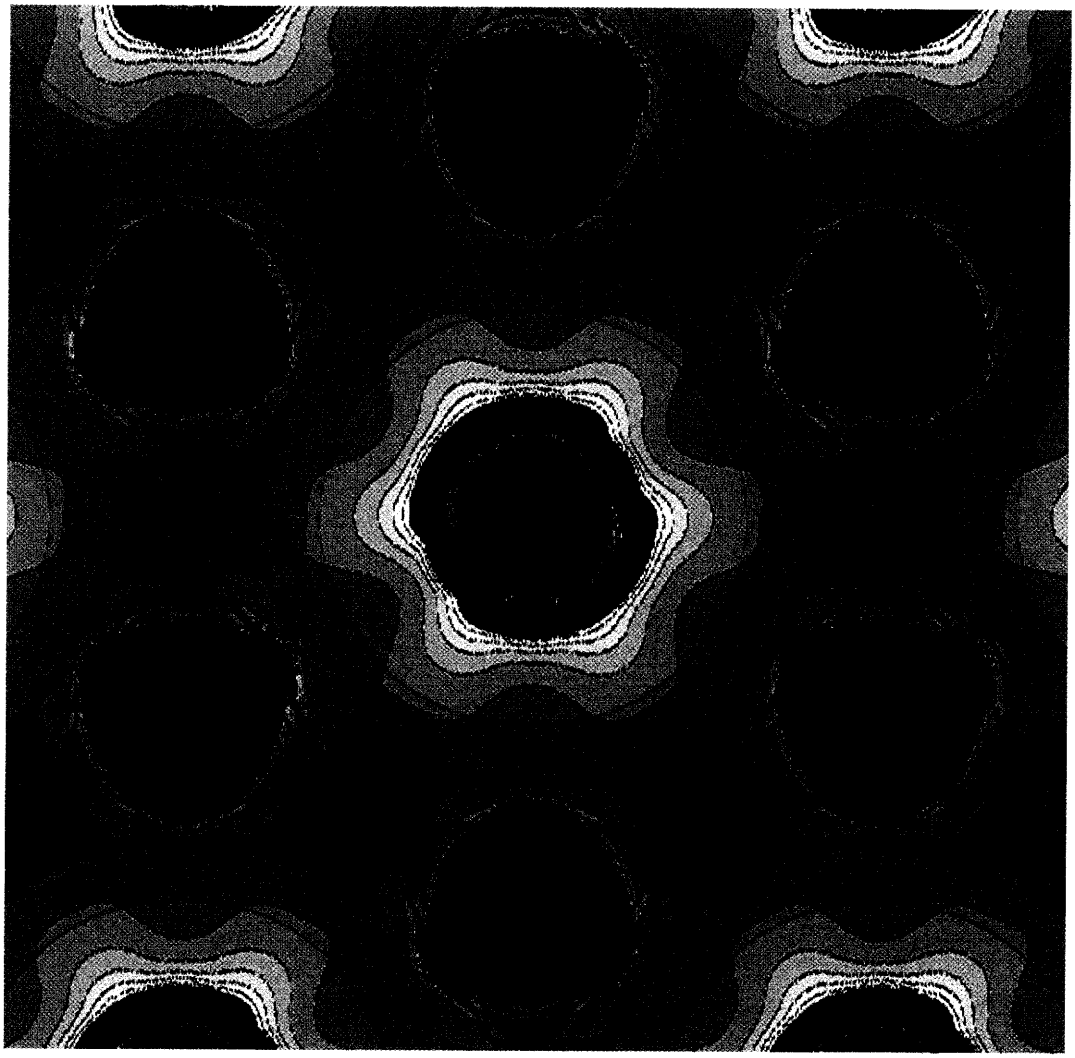

Figure 3.1-7: Overlay of $|K_{2f,10}(q1, q2)|$ for laser energy $2.50eV$ on the 1st nearest neighbor phonon dispersion. The resonant contributions are highlighted in red. (Ignore the solid lines in red.)

As is clear from the above Figure 3.1-6 and Figure 3.1-7, in going from an excitation energy of $2\ eV$ to $2.5\ eV$ we see the highly resonant trigonal ring (highlighted in *red*) around the K point expand to give us a change in the q vectors selected for resonance in the Raman Spectra thereby explaining the shift in the Raman spectra with changing excitation energy.

3.1.4 Raman Spectra of graphene for various excitation energies

The following plots show the Raman spectra of graphene based on our calculations with progressively increasing excitation energies.

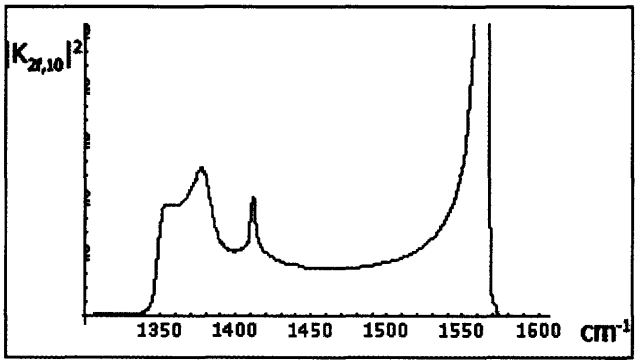

Figure 3.1-8: Raman spectra of graphene with incoming laser energy: 2.00eV

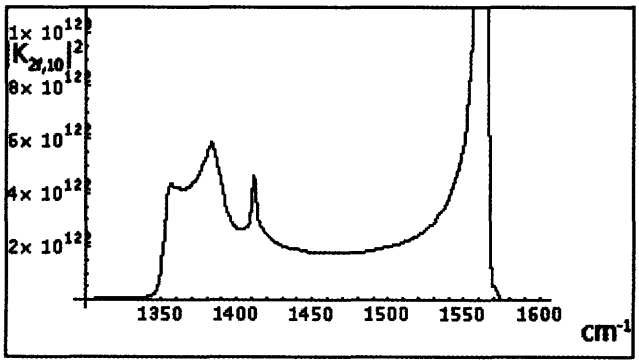

Figure 3.1-9: Raman spectra of graphene with incoming laser energy: 2.10eV

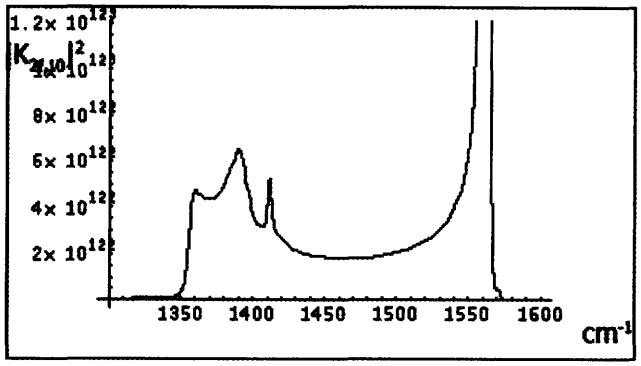

Figure 3.1-10: Raman spectra of graphene with incoming laser energy: 2.20eV

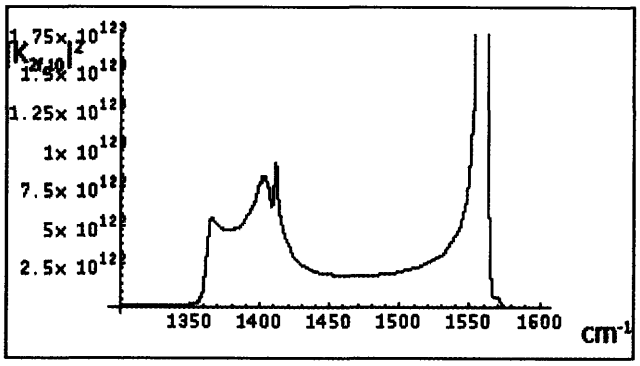

Figure 3.1-11: Raman spectra of graphene with incoming laser energy: 2.40eV

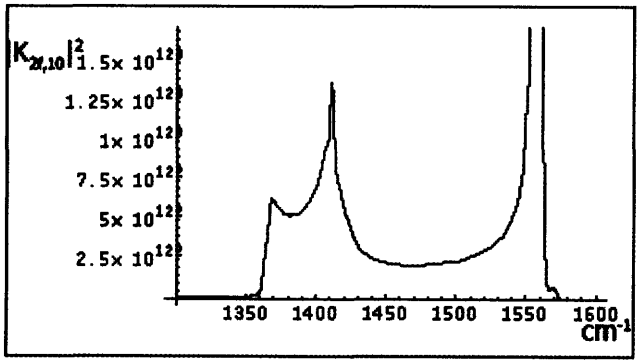

Figure 3.1-12: Raman spectra of graphene with incoming laser energy: 2.50eV

The Raman spectra plotted in Figure 3.1-8 till Figure 3.1-12 shows the presence of an stationary Γ band peak at ~1560 $cm^{-1}$and two peaks that we may associate with the D mode. The peak at ~1360 cm^{-1} does not shift with excitation energy while the higher energy peak shows a near-linear shift with excitation laser energy expected of the D mode.

3.2 Results of calculation with 3rd nearest neighbor phonon dispersion

3.2.1 Electronic band structure used for calculation

This calculation used an electronic band structure identical to the calculation for the spectra for the 1st nearest neighbor interaction and will not be repeated here. Please see section 2.1 for details.

3.2.2 Phonon dispersion used for calculation

The phonon dispersion used for this case was fitted to the Electronic Dispersion obtained with the assumption of up to the 3rd nearest neighbor interaction. The results were given in section 2.1.2 and are being reproduced here for convenience.

$$E(\boldsymbol{k})^{\pm} = \frac{-(-2E_0 + E_1) \mp \sqrt{(-2E_0 + E_1)^2 - 4E_2E_3}}{2E_3} \qquad 3.2.1$$

where

$$E_0 = (\varepsilon_{2p} + \gamma_1 u(k_1, k_2))[1 + s_1 u(k_1, k_2)] \qquad 3.2.1$$

$$E_1 = 2s_0\gamma_0 f_{12}(k_1,k_2) + (s_0\gamma_2 + s_2\gamma_0)g_{12}(k_1,k_2) + 2s_2\gamma_2 f_{12}(2k_1,2k_2) \quad 3.2.2$$

$$E_2 = (\varepsilon_{2p} + \gamma_1 u(k_1,k_2))^2 - {\gamma_0}^2 f_{12}(k_1,k_2) - \gamma_0\gamma_2 g_{12}(k_1,k_2) - {\gamma_2}^2 f_{12}(2k_1,2k_2) \quad 3.2.3$$

$$E_2 = (1 + s_1 u(k_1,k_2))^2 - {s_0}^2 f_{12}(k_1,k_2) - s_0 s_2 g_{12}(k_1,k_2) - {s_2}^2 f_{12}(2k_1,2k_2) \quad 3.2.4$$

Where

$$g_{12}(k_1,k_2) = 2\,u(k_1,k_2) + u(2k_1 - k_2, k_1 - 2k_2) \quad 3.2.5$$

Just as in section 3.1.2 the constants were fitted to inelastic X-ray scattering performed by Maultzsch et al from Ref. (22) for the TO branch as required by symmetry arguments of section 2.4. The values of the constant obtained on fitting the date were obtained as:

$$\varepsilon_{2p} = 0.1718074 * 8065.5\ cm^{-1} \quad \gamma_2 = 0.0032354 * 8065.5\ cm^{-1}$$
$$\gamma_0 = -0.002249 * 8065.5\ cm^{-1} \quad s_1 = s_2 = s_3 = 0$$
$$\gamma_1 = 0.0035423 * 8065.5\ cm^{-1} \quad 3.2.1$$

The plot of phonon energy in units of cm^{-1} is given in Figure 3.2-1 below

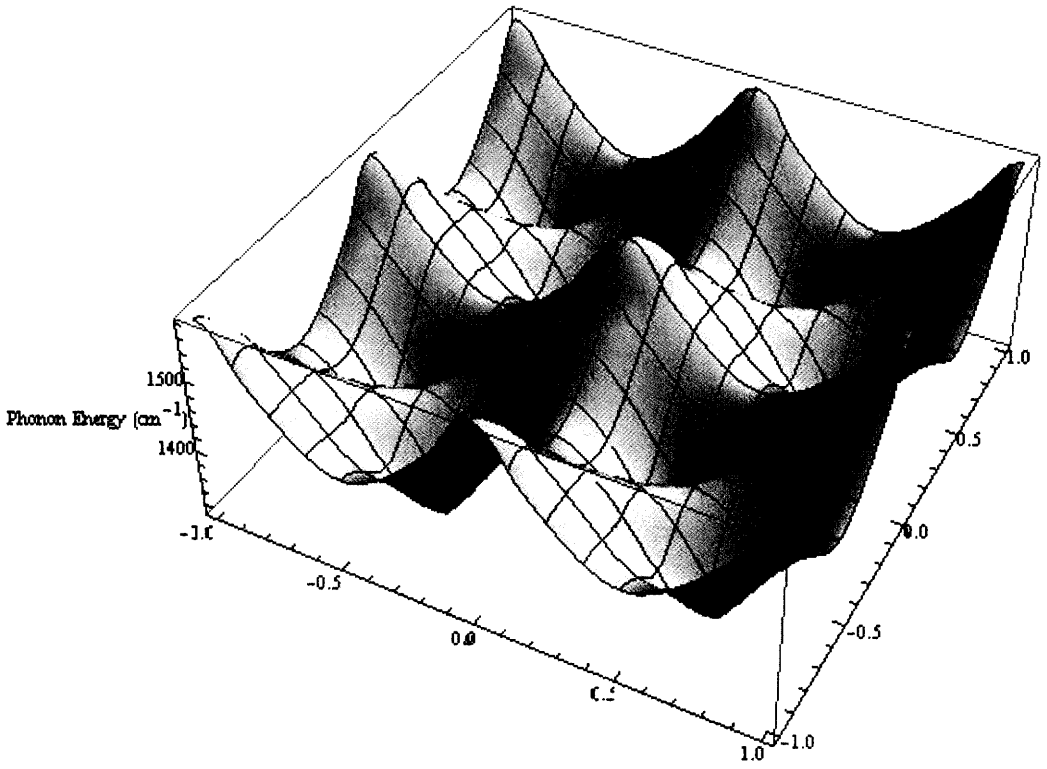

Figure 3.2-1: 3rd nearest neighbor phonon dispersion for graphene

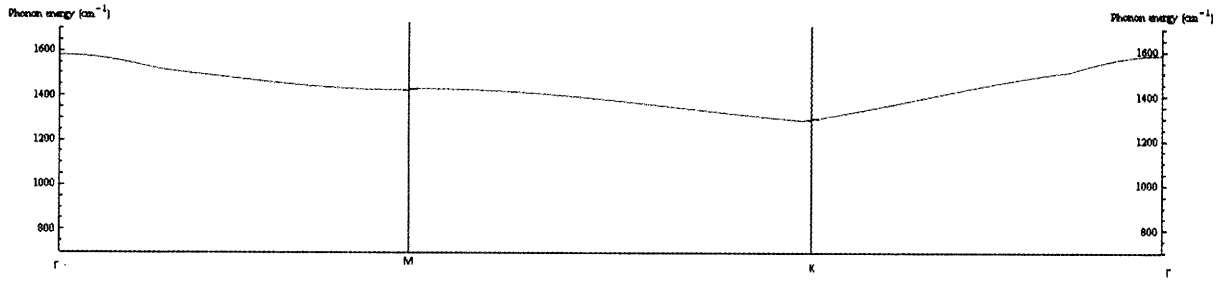

Figure 3.2-2: $\Gamma - K - M$ Phonon Dispersion of Graphene based on the 1st nearest neighbor interaction

3.2.3 Raman spectra of graphene for various excitation energies

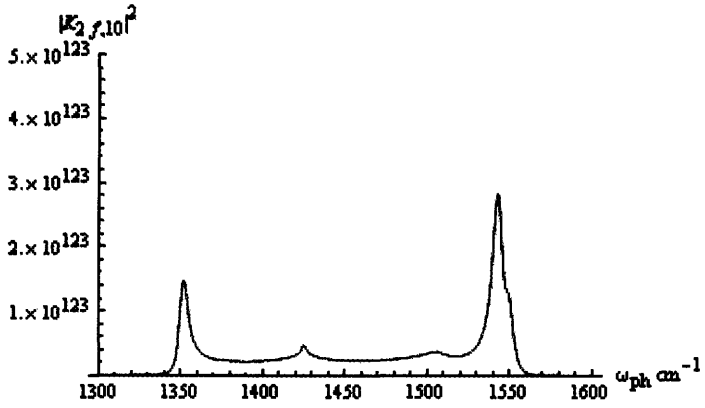

Figure 3.2-3: Raman spectra of graphene with incoming laser energy: 1.90eV

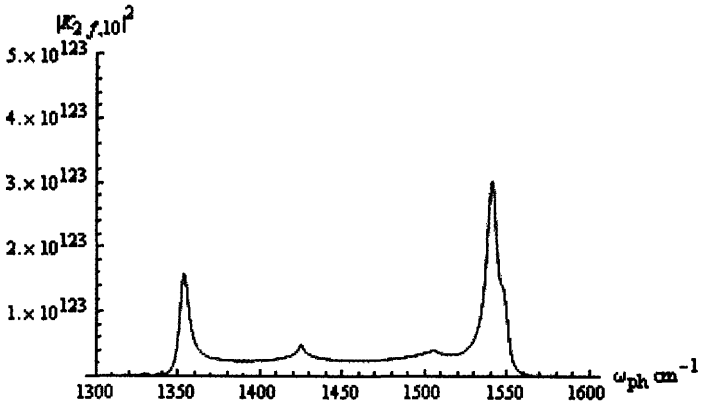

Figure 3.2-4: Raman spectra of graphene with incoming laser energy: 1.95eV

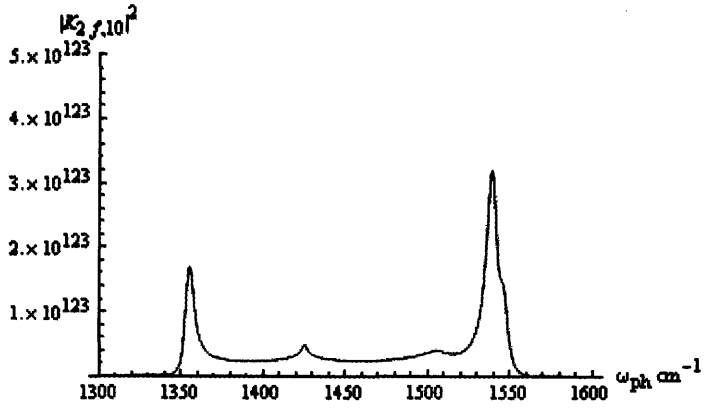

Figure 3.2-5: Raman spectra of graphene with incoming laser energy: 2.00eV

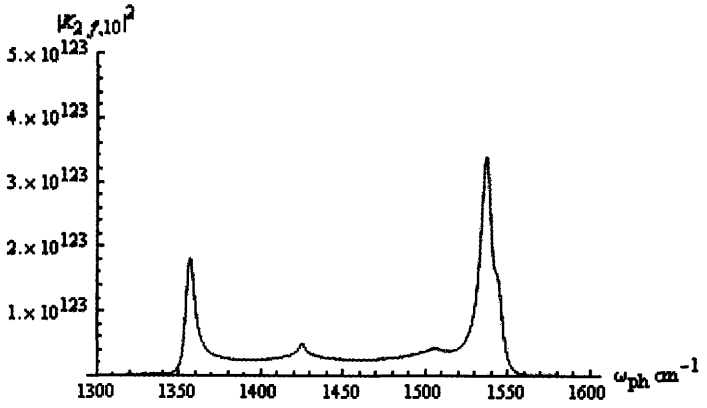

Figure 3.2-6: Raman spectra of graphene with incoming laser energy: 2.05eV

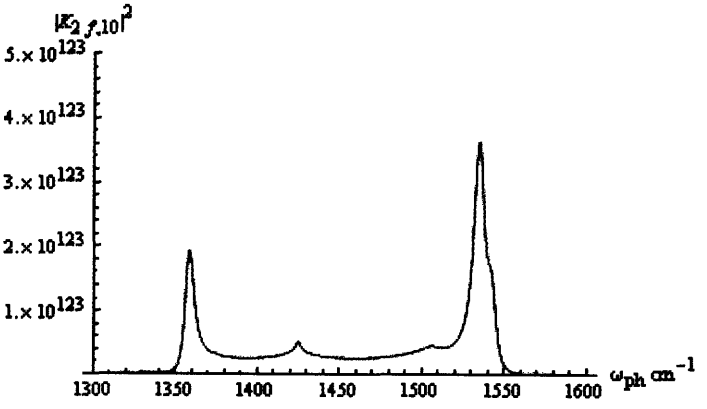

Figure 3.2-7: Raman spectra of graphene with incoming laser energy: 2.10eV

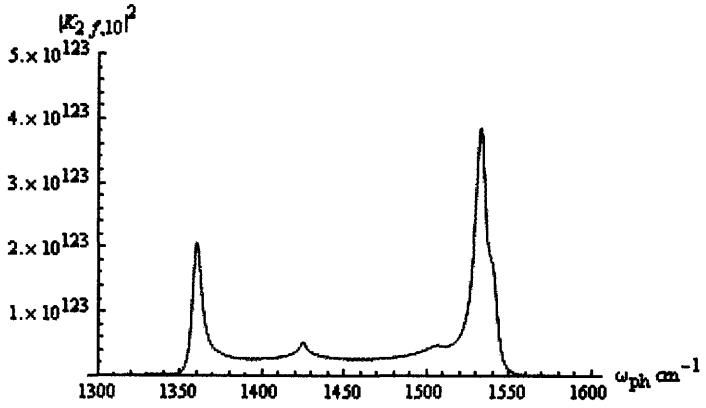

Figure 3.2-8: Raman spectra of graphene with incoming laser energy: 2.15eV

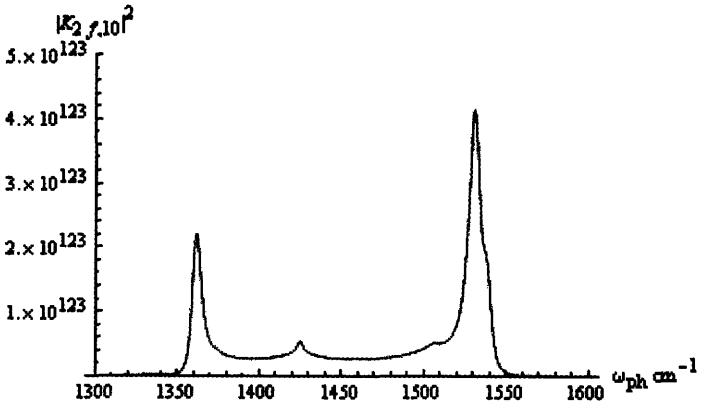

Figure 3.2-9: Raman spectra of graphene with incoming laser energy: 2.20eV

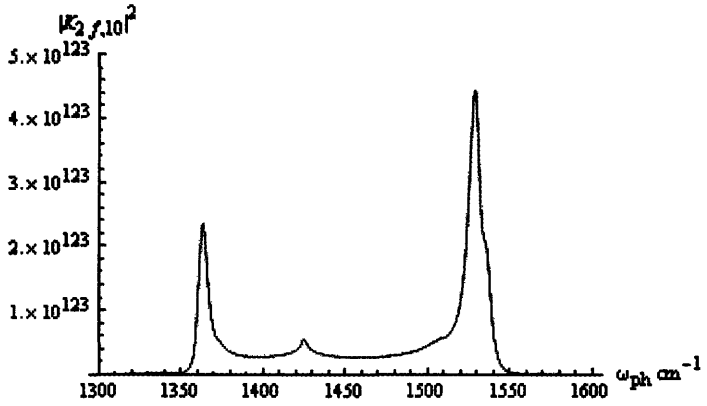

Figure 3.2-10: Raman spectra of graphene with incoming laser energy: 2.25eV

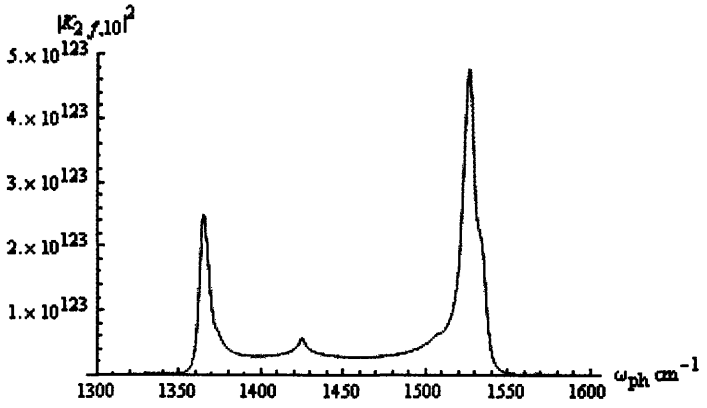

Figure 3.2-11: Raman spectra of graphene with incoming laser energy: 2.30eV

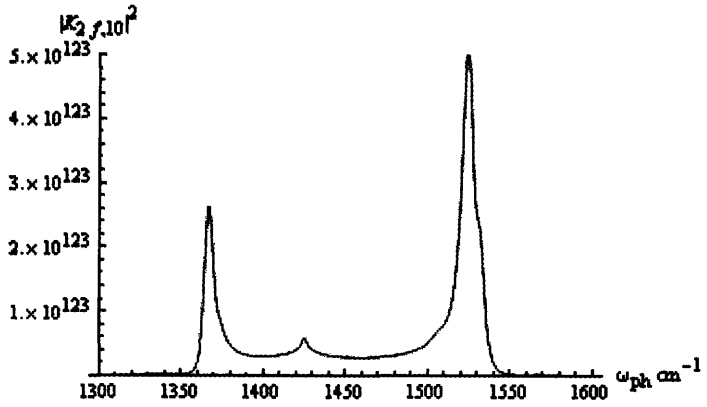

Figure 3.2-12: Raman spectra of graphene with incoming laser energy: 2.35eV

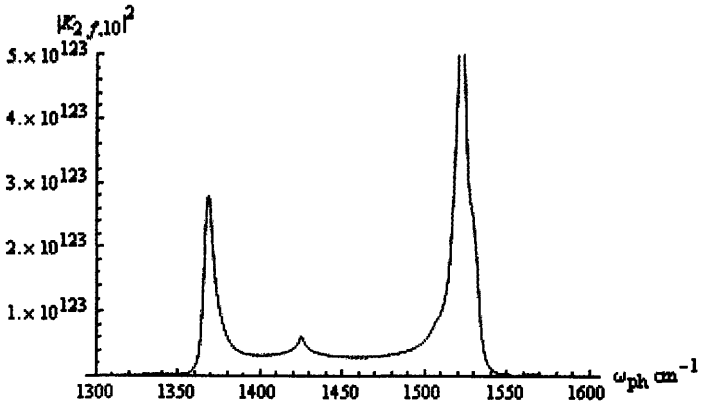

Figure 3.2-13: Raman spectra of graphene with incoming laser energy: 2.40eV

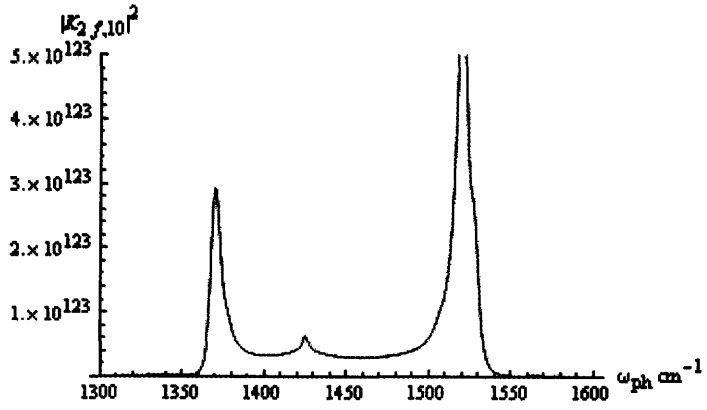

Figure 3.2-14: Raman spectra of graphene with incoming laser energy: 2.45eV

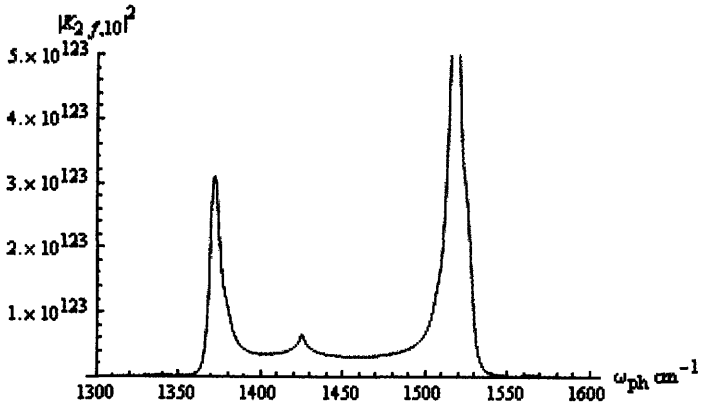

Figure 3.2-15: Raman spectra of graphene with incoming laser energy: 2.50eV

3.2.4 Overlays of $|K_{2f,10}(q_1, q_2)|$ on the phonon dispersion $\omega_{ph}(q_1, q_2)$

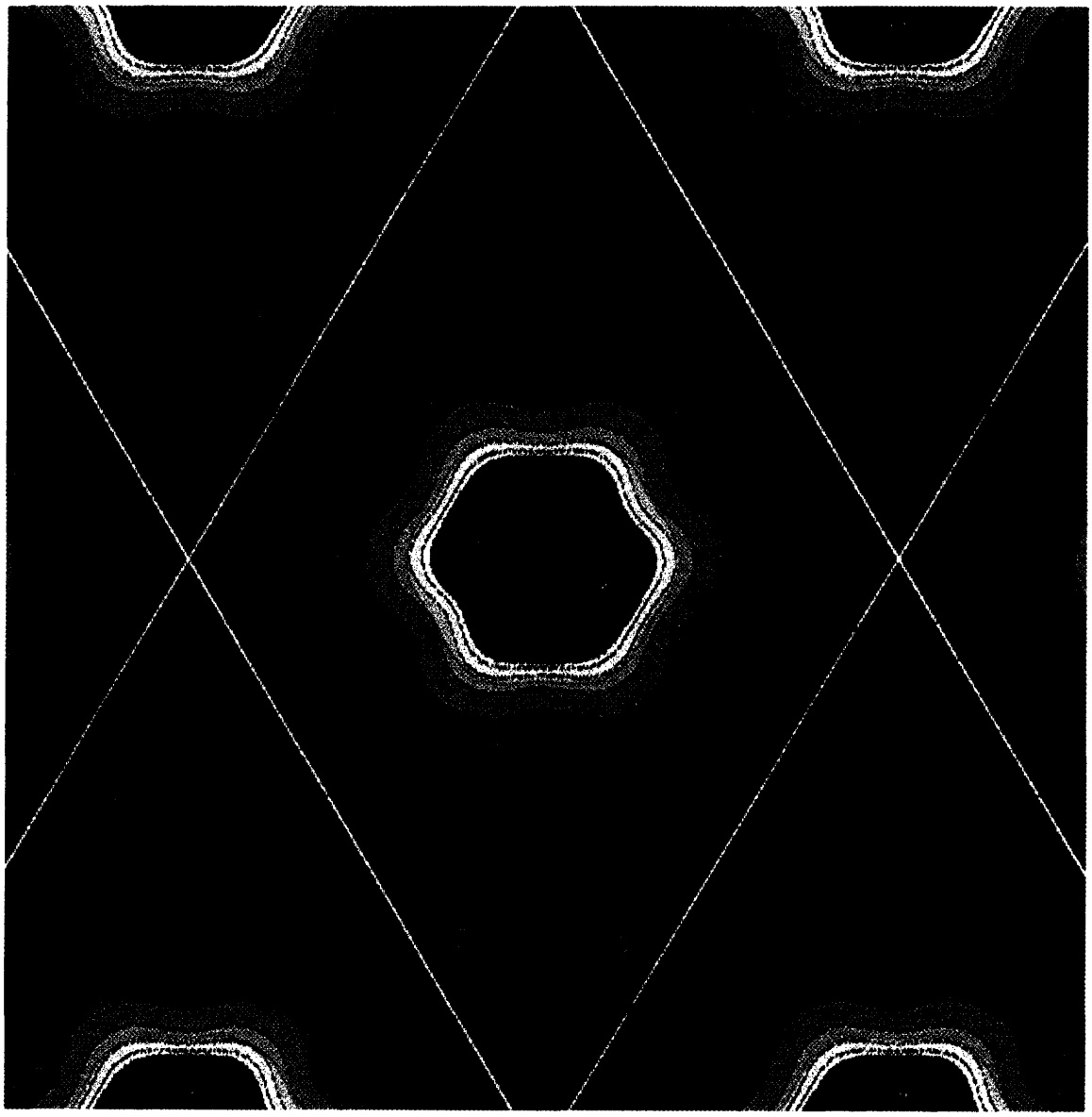

Figure 3.2-16: of $|K_{2f,10}(q1, q2)|$ for laser energy $2.00eV$ on the 3rd nearest neighbor phonon dispersion. The resonant contributions are highlighted in red.

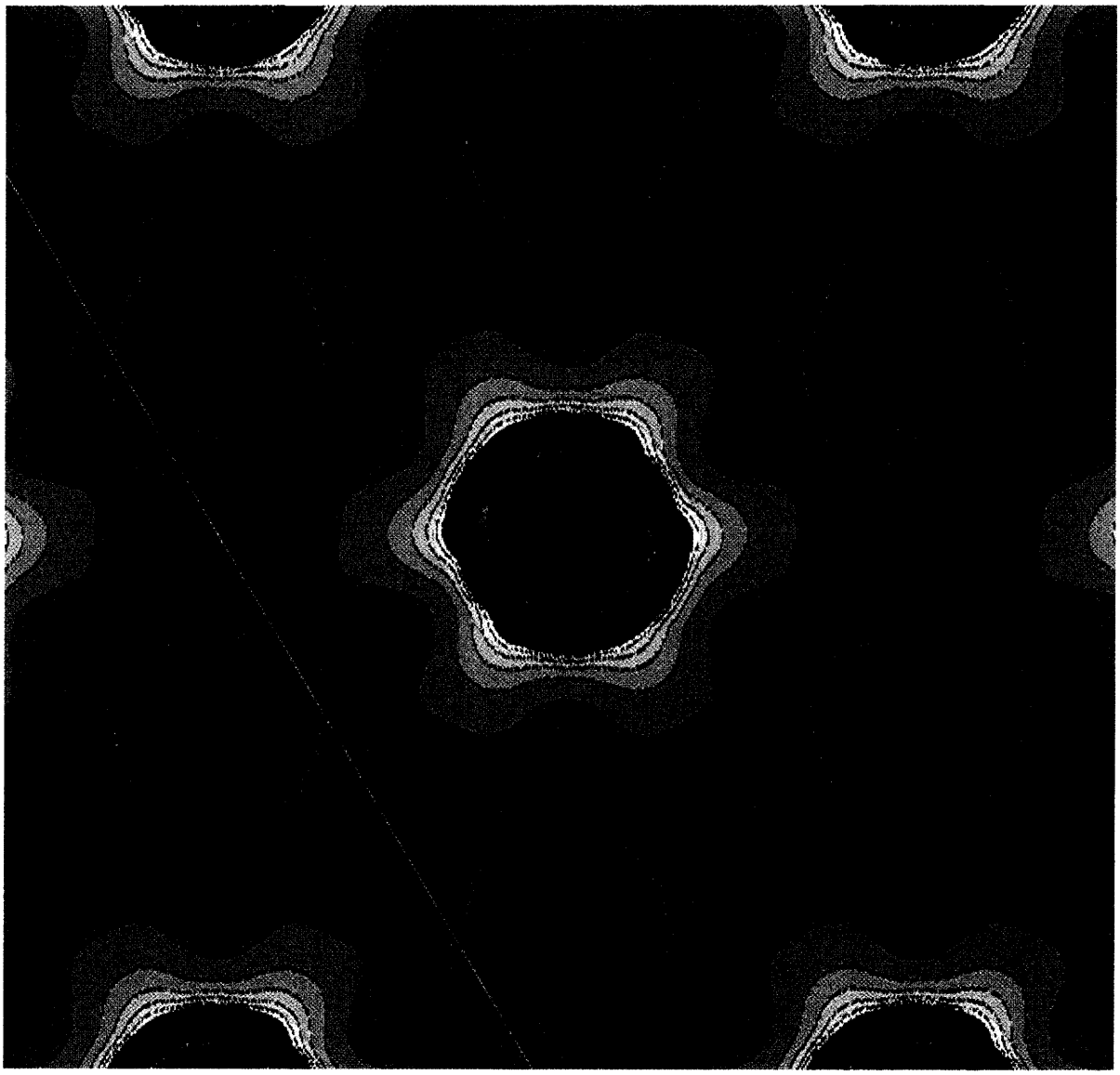

Figure 3.2-17: of $|\kappa_{2f,10}(q_1, q_2)|$ for laser energy 2.50eV on the 3rd nearest neighbor phonon dispersion. The resonant contributions are highlighted in red.

4 Discussion of results and conclusions

4.1 Comparison with experiment

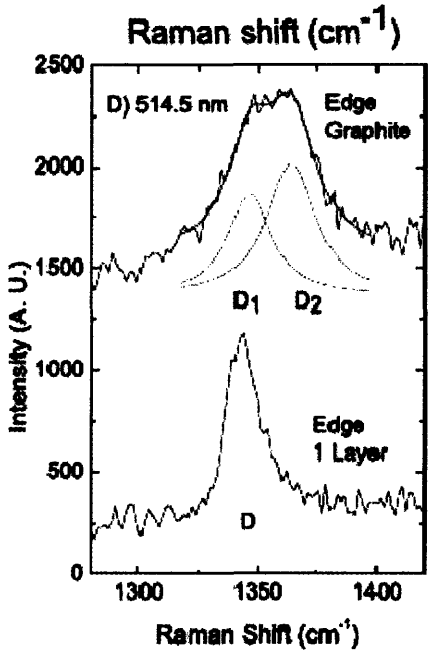

Figure 4.1-1: Experimental Raman spectra of graphite and graphene for excitation laser energy at 514 nm. From Ref. (6).

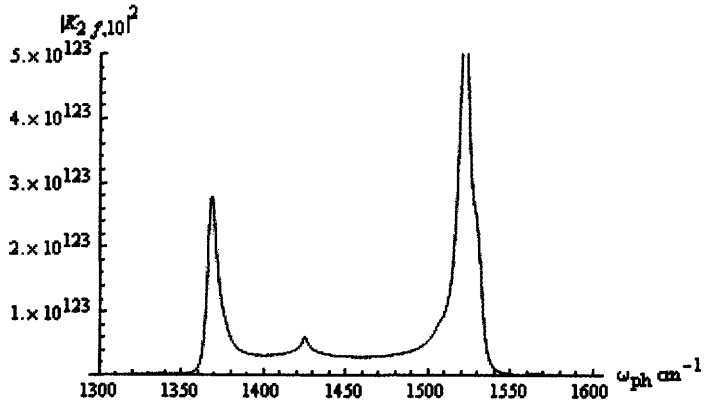

Figure 4.1-2: Raman spectra of graphene with incoming laser energy: 2.40eV, corresponding to the 3rd nearest neighbor phonon dispersion.

Comparing the experimental Raman spectra of graphene of Figure 4.1-1, with the results of our calculation for incoming laser energy 2.40eV (≈ 514 nm) in Figure 4.1-2 we see that our results are able to exactly reproduce the single-peak *D* mode of graphene along with its stronger high-energy flank compared to its lower-energy one! No assumptions regarding which parts of the Brillouin zone contribute to the Raman spectra or arguments involving density of states are made, in contrast to earlier attempts in the literature (See Ref. (6)).

4.2 Shift of Spectra with Change in Laser Energy

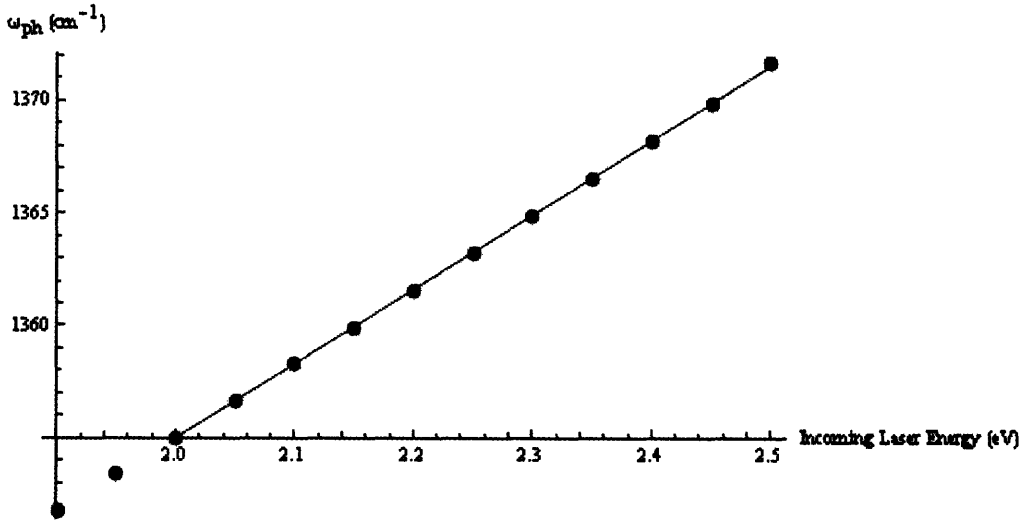

Figure 4.2-1: Near linear shift in the *D* mode of graphene corresponding to a least square value of 33 cm^{-1}/eV

Our numerically obtained spectra are successful in replicating the almost linear shift in D mode peak with change in excitation laser energy (See Figure 4.2-1). The change in the phonon energies corresponding to the D mode peak selected is observed in two dimensions going from the overlays of Figure 3.2-16 to Figure 3.2-17. Clearly, the trigonal ring around the K point is seen to expand outwards with increasing excitation laser energy leading to different phonon energies being selected corresponding to the D peak.

We obtained a shift of 33 cm^{-1}/eV which is comparable to the experimentally obtained shift of roughly 40-50 cm^{-1}/eV depending on the publication and the exact *flavor* of multi-layer graphene/graphite used. Nevertheless, we must note that the experimental spectra of single-layer graphene has never been measured for a range of excitation energies. Therefore, any subsequent discrepancy may be explained in part by the changing atomic structure experienced by progressively stacking layer upon layer of graphene that finally results in graphite. The interplanar interaction between the carbon atoms is likely to change the tight binding expression obtained in section 2.1, and hence the corresponding electronic

band structure and phonon dispersion. Another possibility is that we have used the phonon dispersion of graphite (22), instead of that for graphene.

However, our results regarding the absolute phonon wave numbers at which the D mode exists are slightly off from experiment. This may again be attributed to using an incorrect phonon dispersion in our calculation.

4.3 *M* Point Peak in Numerically Obtained Spectra

Comparing Figure 4.1-1 and Figure 4.1-2 we clearly see the presence of both the *D* mode and the *Γ* mode in both the spectra. However, a small peak corresponding at phonon energy 1425 cm^{-1} is missing for the experimental spectra. It's presence in Figure 3.2-3 till Figure 3.2-15 of our results stems from the fact that the phonon dispersion of graphene contains a *Van Hove singularity* of the type M_1 in two dimensions (also known as a saddle-point) at its *M* point (See Figure 4.3-1). Indeed, we fitted the *M* point of graphene exactly at the value of 1425 cm^{-1} for the 3rd nearest neighbor phonon dispersion and therefore we see a peak at that energy in our results. Yet, this peak is absent from the experimental results of Ref. (17), as the *M* point is selection-rule limited. See Ref. (24).

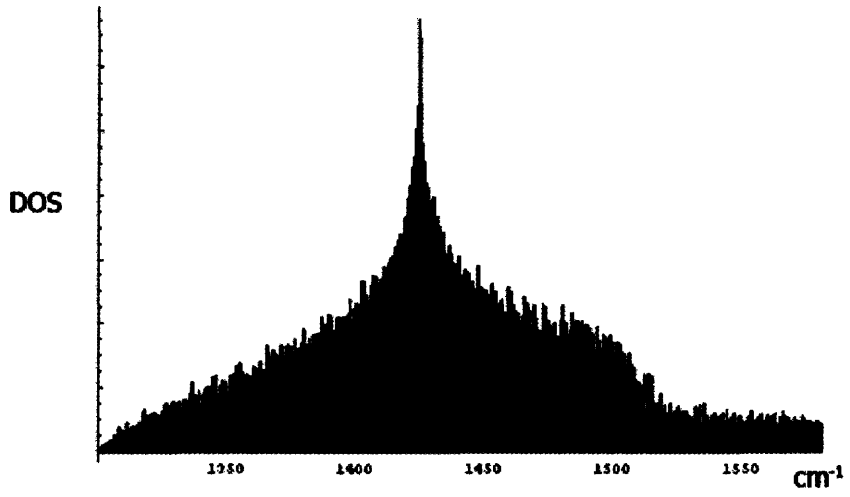

Figure 4.3-1: Type M_1 Van Hove singularity (saddle point) present at 1425 cm^{-1} in the 3rd nearest neighbor phonon dispersion of graphene corresponding to the *M* point.

4.4 Differences between the one dimensional and two dimensional calculations

As is shown in Figure 2.3-6, the one dimensional calculation leads to a double peak structure for the *D* mode peak whereas our two dimensional calculation results in a single peak with a stronger high-energy flank than the low-energy one for the *D* mode that is observed experimentally.

4.5 Inadequacy of the 1st nearest neighbor phonon dispersion

The fitting of the 1st nearest neighbor tight binding expression to the phonon dispersion of graphite (as per Ref. (22)) was unable to achieve the correct trigonal warping around the *K* point. This resulted in the odd double-peak structure of the

D mode of the Raman spectra with one stationary peak and while the other showed a familiar near-linear shift with changing excitation energy.

4.6 Scope for Future Work

- Having calculated the Raman spectra for graphene, our 2-D model provides ready extensibility to multi layered versions of graphene through to graphite. All we need to specify in our calculation is the modified tight binding expressions for the electronic bands and the phonon dispersions that shows band-splitting and opening up of an electronic band gap at the K point. This will allow us to study the changes in the peak structure of the D mode with increasing number of layers such as the eventual double-peak structure observed experimentally for graphite.
- Calculate the second order spectra of graphene based on our model associated with the D^* mode and compare with experiment.
- Measure the Raman spectra of graphene experimentally for a range of excitation energies.
- Calculate all the matrix elements in the expression for $K_{2f,10}$ except for the one involving the defect scattering.

4.7 Conclusions

Our results are able to replicate the near linear shift of the D mode in the Raman spectra of graphene (when compared to graphene) with changing excitation laser energy of 33 cm^{-1}/eV. This compares favorably with experimental data on graphite. Without resorting to any ad hoc assumptions our calculations neatly reproduce the single peak structure of the D mode that distinguishes the spectra of graphene from the double-peak D mode of graphite.

The false peak corresponding to the M point frequency (1425 cm^{-1}) is merely an artifact of our calculation and can easily be precluded based on selection rule restrictions.

Our methodology to produce Raman spectra may be easily extended to multi layer graphene, graphite and carbon nanotubes by suitably adjusting the tight binding expression used to generate the electronic and phonon dispersions.

5 Appendix

5.1 Mathematica code to generate $K_{2f,10}(q_1, q_2)$ for the 1st nearest neighbor phonon dispersion

```
Needs["Parallel`Debug`"]
Needs["Parallel`"]
Print[Date[]];
inc2 = 1
inc1 = 10
CloseSlaves[];
LaunchSlave["hofstadter"];
LaunchSlave["achilles"];
LaunchSlave["tortoise"];
LaunchSlave["crab"];
(*Constants*)
h = 6.636 * 10^-34 / (2 π);
e = 1.602 * 10^-19;
E1 = (2 + inc1 * 0.05) * e;
Print["Calculating....." <> ToString[(2 + inc1 * 0.05)] <> "eV" <> ToString[(inc2 / 10)] <> "b"];
b = (inc2 / 10) * e;
γ0 = 2.84 * e;
s0 = 0.07;
su1 := 0;
su2 := 0;
(*Tight Binding Description of Electronic Bands*)
f12[u_, v_] := 3 + 2 Cos[2 π * u] + 2 Cos[2 π * v] + 2 Cos[2 π * (u - v)];
E1[u_, v_] := (-γ0 Sqrt[f12[u, v]]) / (1 + s0 Sqrt[f12[u, v]]);
E2[u_, v_] := (+γ0 Sqrt[f12[u, v]]) / (1 - s0 Sqrt[f12[u, v]]);
Ea1[u_, v_] := E2[u, v] - E1[u, v];
Eb11[u_, v_] := E2[u - q1, v - q2] - E1[u, v];
Eb12[u_, v_] := E2[u + q1, v + q2] - E1[u, v];
fu[u_, v_] :=
  1/((E1 - Ea1[u, v] - h * b)
     (E1 - ((0.155 * e + 0.0783333 * e * Sqrt[3 + 2 Cos[2 π * q1] + 2 Cos[2 π * q2] + 2 Cos[2 π * (q1 - q2)]])/
        (1 + 0.333333 * Sqrt[3 + 2 Cos[2 π * q1] + 2 Cos[2 π * q2] + 2 Cos[2 π * (q1 - q2)]])) - Eb11[u, v] - h * b)
     (E1 - ((0.155 * e + 0.0783333 * e * Sqrt[3 + 2 Cos[2 π * q1] + 2 Cos[2 π * q2] + 2 Cos[2 π * (q1 - q2)]])/
        (1 + 0.333333 * Sqrt[3 + 2 Cos[2 π * q1] + 2 Cos[2 π * q2] + 2 Cos[2 π * (q1 - q2)]])) - Ea1[u, v] - h * b)) +
  1/((E1 - Ea1[u, v] - h * b) (E1 - Eb12[u, v] - h * b)
     (E1 - ((0.155 * e + 0.0783333 * e * Sqrt[3 + 2 Cos[2 π * q1] + 2 Cos[2 π * q2] + 2 Cos[2 π * (q1 - q2)]])/
        (1 + 0.333333 * Sqrt[3 + 2 Cos[2 π * q1] + 2 Cos[2 π * q2] + 2 Cos[2 π * (q1 - q2)]])) - Ea1[u, v] - h * b));
MemoryInUse[];
(*Determining Functional Dependence of K2f,10 on q1,q2*)
Do[su1 += Evaluate[fu[u, v]], {v, 0, 0.5, 0.0025}];
Do[su2 += Evaluate[su1], {u, -0.5, 0.5, 0.0025}];
MemoryInUse[];
su3 = ParallelTable[Evaluate[Abs[su2]], {q2, -0.5, 0, 0.0025}, {q1, -0.5, 0.5, 0.0025}];
Export["parallel" <> ToString[(2 + inc1 * 0.05) * 100] <> "eV" <> ToString[inc2] <> "b" <> ".csv", TableForm[su3], "CSV"];
Print[Date[]];
Clear[su1, su2, su3, fu];
Abort[];
```

5.2 Mathematica code to generate $K_{2f,10}(q_1, q_2)$ for the 3rd nearest neighbor phonon dispersion

```
Needs["Parallel`Debug`"]
Needs["Parallel`"]
Print[Date[]];
inc2 = 1
inc1 = 20
(*Constants*)
h = (6.636 * 10^-34) / (2 π);
e = 1.602 * 10^-19;
E1 = (2 + inc1 * 0.05) * e;
Print["Calculating....." <> ToString[(2 + inc1 * 0.05)] <> "eV" <> ToString[(inc2 / 10)] <> "b"];
b = (inc2 / 10) * e;
γE0 = 2.84 * e;
sE0 = 0.07;
su1 := 0;
su2 := 0;
(*Tight Binding Description of Electronic Bands*)
Ei = Compile[{{u, _Real}, {v, _Real}}, (-γE0 * Abs[Sqrt[3 + 2 Cos[2 π * u] + 2 Cos[2 π * v] + 2 Cos[2 π * (u - v)]]]) /
    (1 + sE0 * Abs[√(3 + 2 Cos[2 π * u] + 2 Cos[2 π * v] + 2 Cos[2 π * (u - v)])])];
Ex = Compile[{{u, _Real}, {v, _Real}}, (+γE0 * Abs[Sqrt[3 + 2 Cos[2 π * u] + 2 Cos[2 π * v] + 2 Cos[2 π * (u - v)]]]) /
    (1 - sE0 * Abs[√(3 + 2 Cos[2 π * u] + 2 Cos[2 π * v] + 2 Cos[2 π * (u - v)])])];
Eai = Compile[{{u, _Real}, {v, _Real}}, Ex[u, v] - Ei[u, v]];
Ebi1 = Compile[{{u, _Real}, {v, _Real}, {q1, _Real}, {q2, _Real}}, Ex[u - q1, v - q2] - Ei[u, v]];
Ebi2 = Compile[{{u, _Real}, {v, _Real}, {q1, _Real}, {q2, _Real}}, Ex[u + q1, v + q2] - Ei[u, v]];
ε2p = 0.17180742020168557`;
γ0 = -0.00224931805514005`;
γ1 = 0.0035423640675591467`;
γ2 = 0.0032354757026555538`;
u12 = Compile[{{u, _Real}, {v, _Real}}, 2 Cos[2 π * u] + 2 Cos[2 π * v] + 2 Cos[2 π * (u - v)]];
f12 = Compile[{{u, _Real}, {v, _Real}}, 3 + 2 Cos[2 π * u] + 2 Cos[2 π * v] + 2 Cos[2 π * (u - v)]];
g12 = Compile[{{u, _Real}, {v, _Real}}, 2 * u12[u, v] + 2 Cos[2 π * (2 * u - v)] + 2 Cos[2 π * (u - 2 * v)] + 2 Cos[2 π * (2 * u - v - u + 2 * v)]];
E0 = Compile[{{u, _Real}, {v, _Real}}, (ε2p + γ1 * u12[u, v])];
E2 = Compile[{{u, _Real}, {v, _Real}}, (ε2p + γ1 * u12[u, v]) ^2 - γ0^2 * f12[u, v] - γ0 * γ2 * g12[u, v] - γ2^2 * f12[2 u, 2 v]];
ω = Compile[{{u, _Real}, {v, _Real}}, e / 2 (-(-2 E0[u, v]) + Abs[√((-2 E0[u, v]) ^2 - 4 E2[u, v])])];
fu1 = Compile[{{u, _Real}, {v, _Real}, {q1, _Real}, {q2, _Real}}, 1 / ((E1 - Eai[u, v] - ħ * b) (E1 - ω[q1, q2] - Ebi1[u, v, q1, q2] - ħ * b) (E1 - ω[q1, q2] - Eai[u, v] - ħ * b)),
  {{fu, _Complex}}];
a1 = Sum[fu1[u, v, q1, q2], {u, -0.5, 0.5, 0.0025}, {v, 0, 0.5, 0.0025}];
Print[MemoryInUse[]];
bb1 = ParallelTable[Evaluate[a1], {q1, -0.5, 0.5, 0.0025}, {q2, -0.5, 0, 0.0025}];
TableForm[bb1]
Print[MemoryInUse[]];
Export["compile-300ev-first-complex-timeorder-final.csv", bb1];
Clear[a1, fu1];
fu2 = Compile[{{u, _Real}, {v, _Real}, {q1, _Real}, {q2, _Real}}, 1 / ((E1 - Eai[u, v] - ħ * b) (E1 - Ebi2[u, v, q1, q2] - ħ * b) (E1 - ω[q1, q2] - Eai[u, v] - ħ * b)),
  {{fu, _Complex}}];
a2 = Sum[fu2[u, v, q1, q2], {u, -0.5, 0.5, 0.0025}, {v, 0, 0.5, 0.0025}];
Print[MemoryInUse[]];
bb2 = ParallelTable[Evaluate[a2], {q1, -0.5, 0.5, 0.0025}, {q2, -0.5, 0, 0.0025}];
TableForm[bb2]
Print[MemoryInUse[]];
Export["compile-300ev-second-complex-timeorder-final.csv", bb2];
Clear[a2, fu2];
CloseSlaves[];
final = TableForm[Abs[bb1 + bb2]]
Export["compile-300ev-complete-absolute-timeorder-final.csv", final, "CSV"]
```

5.3 Code to generate Raman spectra

```
Print[Date[]];
σ = 1;
gaussian[y_] := e^(-(x - y)^2 / (2 σ^2))
ε2p = 0.17180742820168557`;
γ0 = -0.80224931885514805`;
γ1 = 0.80354236486755914467`;
γ2 = 0.80323547570265555380`;
u12 = Compile[{{u, _Real}, {v, _Real}}, 2 Cos[2 π * u] + 2 Cos[2 π * v] + 2 Cos[2 π * (u - v)]];
f12 = Compile[{{u, _Real}, {v, _Real}}, 3 + 2 Cos[2 π * u] + 2 Cos[2 π * v] + 2 Cos[2 π * (u - v)]];
g12 = Compile[{{u, _Real}, {v, _Real}}, 2 * u12[u, v] + 2 Cos[2 π * (2 * u - v)] + 2 Cos[2 π * (u - 2 * v)] + 2 Cos[2 π * (2 * u - v - u + 2 * v)]];
E0 = Compile[{{u, _Real}, {v, _Real}}, (ε2p + γ1 * u12[u, v])];
E2 = Compile[{{u, _Real}, {v, _Real}}, (ε2p + γ1 * u12[u, v]) ^2 - γ0^2 * f12[u, v] - γ0 * γ2 * g12[u, v] - γ2^2 * f12[2 u, 2 v]];
ω = Compile[{{u, _Real}, {v, _Real}}, 8865.5 / 2 (-(-2 E0[u, v]) + Abs[√((-2 E0[u, v])^2 - 4 E2[u, v])])];
For[inc = -2, inc ≤ 10, inc = inc + 1,
  Clear[aa1];
  aa1 = Import["3nn-full-" <> ToString[200 + inc * 5] <> "ev.csv", "CSV"];
  su = Evaluate[Sum[aa1[[q1, q2]]^2 * gaussian[ω[(q1 - 201) / 400, (q2 - 201) / 400]], {q1, 1, 401}, {q2, 1, 401}]];
  Export["plotsum" <> ToString[200 + inc * 5] <> ".txt", su];
  Print["Printing....." <> ToString[200 + inc * 5] <> "eV"];
  Print[Plot[su, {x, 1300, 1600}, PlotRange → {0, 5 * 10^123}]];
  Clear[su];
  Print[Date[]]];
```

6 Bibliography

1. *Electric Field Effect in Atomically Thin Carbon Films.* **Novoselov, K S, et al.** 5696, s.l. : AAAS, 2001, Science, Vol. 306, pp. 666-669.

2. *Energy gaps in zero-dimensional graphene nanoribbons.* **Shemella, P, et al.** 2007, Appl. Phys. Lett. , Vol. 91, p. 042101.

3. *Two-dimensional gas of massless Dirac fermions in graphene.* **Novoselov, K S et al.** 2005, Nature, Vol. 438, pp. 197-200.

4. *Double-Resonant Raman Scattering in Graphite.* **Thomsen, C and Reich, S.** 2000, Phys. Rev. Lett., Vol. 85, p. 5214.

5. *Double-resonant Raman Scattering in Graphite: Interference Effects, Selection Rules, and Phonon Dispersion.* **Maultzsch, J, Reich, S and Thomsen, C.** 2004, Phys. Rev. B, Vol. 70, p. 155403.

6. *The Raman Fingerprint of Graphene.* **Ferrari, A C, et al.** s.l. : cond-mat-Arxiv, 2006.

7. *Ab Initio Calculations of the Optical Properties of 4A-diameter Single-Walled Carbon Nanotubes.* **Machon, M., et al.** 2002, Phys. Rev. B, Vol. 66, p. 155410.

8. **Reich, S, Thomsen, C and Maultzsch, J.** *Carbon Nanotubes: Basic Concepts and Physical Properties.* s.l. : Wiley-VCH, 2004.

9. *Tight Binding Description of Graphene.* **Reich, S, et al.** 2002, Phys. Rev. B, Vol. 66, p. 035412.

10. **Yu, Peter Y and Cardona, Manuel.** *Fundamentals of Semiconductors.* s.l. : Springer-Verlag, 1999.

11. **Cohen-Tannoudji, C, Dupont-Roc, J and Grynberg, G.** *Atom-Phonon Interactions.* s.l. : John Wiley & Sons. Inc., 1992.

12. *Brillouin Scattering Measurements on Silicon and Germanium.* **Sandercock, J R.** 1972, Phys. Rev. Lett., Vol. 8, pp. 237-240.

13. *Light Scattering from Surface Acoustic Phonons in Metals and Semiconductors.* **Sandercock, J R.** 1978, Solid State Commun., Vol. 26, pp. 547-551.

14. *Raman Scattering in Carbon Nanotubes Revisited.* **Maultzsch, J, Reich, S and Thomsen, C.** 2002, Phys. Rev. B, Vol. 65, p. 233402.

15. *Chirality-Selective Raman Scattering f the D mode in Carbon Nanotubes.* **Maultzsch, J, Reich, S and Thomsen, C.** 2001, Phys. Rev. B, Vol. 64, p. 121407.

16. **Martin, R M and Falicov, L M.** Resonant Raman Scattering. [ed.] M Cardona. *Light Scattering in Solids I.* s.l. : Springer-Verlag, 1983, Vol. 8, p. 79.

17. *Origin of D peak in the Raman Spectrum of Microcrystalline Graphite.* **Pocsik, I, et al.** 1998, J. of Non Cryst. Solids, Vols. 227-230, pp. 1083-1086.

18. *Raman Spectroscopy of Carbon Materials: Structural Basis of Observed Spectra.* **Wang, Y, Alsmeyer, D and McCreery, R.** 1990, Vol. 2, pp. 557-563.

19. *Fundamentals, overtones, and combinations in the Raman spectrum of graphite.* **Kawashima, Y and Katagiri, G.** 1995, Phs. Rev. B, Vol. 52, pp. 10053-10059.

20. *Polarization properties, high-order Raman spectra, and frequency asymmetry between Stokes and anti-Stokes scattering of Raman modes in a graphite whisker.* **Tan, P, et al.** 2001, Phys. Rev. B, Vol. 64, p. 214301.

21. *Probing the phonon dispersion relations of graphite from the double-resonance process of Stokes and anti-Stokes Raman scatterings in multiwalled carbon nanotubes.* **Tan, P, An, L and Guo, H.** 2002, Phys. Rev. B, Vol. 66, p. 245410.

22. *Phonon Dispersion in Graphite.* **Maultzsch, J, et al.** 2004, Phys. Rev. Lett., Vol. 92, p. 075501.

23. *The SIESTA method for ab initio order-N materials simulation.* **Soler, J M, et al.** 2002, J. Phys: Condens. Matter, Vol. 14, p. 2745.

24. *Raman spectroscopy of graphite.* **Reich, S and Thomsen, C.** 1824, 2004, Philosophical Transactions of the Royal Society: A, Vol. 362, pp. 2271-2288.

Table of Contents

List of Figures